Analysis Note
of the STAR Experiment

# Supplementary note on diffractive analyses of 2015 proton-proton data:

## [1] Measurement of Central Exclusive Production of $h\bar{h}$ pairs ($h = \pi, K, p$) with Roman Pot detectors in diffractive proton-proton interactions at $\sqrt{s} = 200$ GeV

## [2] Measurement of particle production with Roman Pot detectors in diffractive proton-proton interactions at $\sqrt{s} = 200$ GeV

Leszek Adamczyk[1], Łukasz Fulek[1], and Rafał Sikora[1]

[1] *AGH University of Science and Technology, FPACS, Kraków, Poland*

May 9, 2018

**Abstract**

In this note we present supplementary material related to analyses of diffractive processes based on 2015 data from proton-proton collisions at $\sqrt{s} = 200$ GeV. This dataset was collected with newly installed Roman Pot detectors in Phase II* configuration which ensured efficient triggering and measuring diffractively scattered protons.

We focus on calculation of efficiencies, corrections to Monte Carlo simulations and derivation of systematic uncertainties of our measurements.

# Contents

# 1. Efficiencies

## 1.1 TPC track acceptance and reconstruction efficiency

We define joint acceptance and efficiency of the reconstruction of a track in the TPC, $\epsilon_{\mathrm{TPC}}$, as the probability that particle from the primary interaction generates signal in the detector which is reconstructed as a track that satisfies all quality criteria and whose $p_T$ and $\eta$ are within the kinematic region of the measurement (cuts **??** and **??**).

Thechnically this quantity is derived from STARsim MC embedded into zero-bias triggers in the following procedure:

1. True-level primary particles of given ID and charge, with all physics ($p_T^{\mathrm{true}}$, $\eta^{\mathrm{true}}$) and detector ($z_{\mathrm{vx}}$) quantities within defined region of the measurement, are selected (*set A*).

2. Each particle from *set A* is checked if global TPC track with more than half of hit points generated by this particle, was reconstructed. All global tracks which are associated with true-level primary particles and satisfy kinematic and quality criteria (cuts **??** and **??**), form *set B*.

3. The joint TPC acceptance and efficiency is calculated as the ratio of the histograms of true-level quantities (such as $p_T$, $\eta$, $z_{\mathrm{vx}}$) for particles from *set B* and particles from *set A*:

$$\epsilon_{\mathrm{TPC}}\left(p_T, \eta, z_{vx};\ \mathrm{sign}, \mathrm{PID}\right) = \frac{(p_T, \eta, z_{vx}) \text{ histogram for particles of given sign and ID from } \textit{set B}}{(p_T, \eta, z_{vx}) \text{ histogram for particles of given sign and ID from } \textit{set A}}. \quad (1.1)$$

Figure 1.1: TPC acceptance and reconstruction efficiency of $\pi^-$. Each plot represents the TPC efficiency $\epsilon_{\mathrm{TPC}}$ ($z$-axis) as a function of true particle pseudorapidity $\eta$ ($x$-axis) and transverse momentum $p_T$ ($y$-axis) in single $z$-vertex bin whose range is given at the top. Red lines and arrows indicate region accepted in analyses.

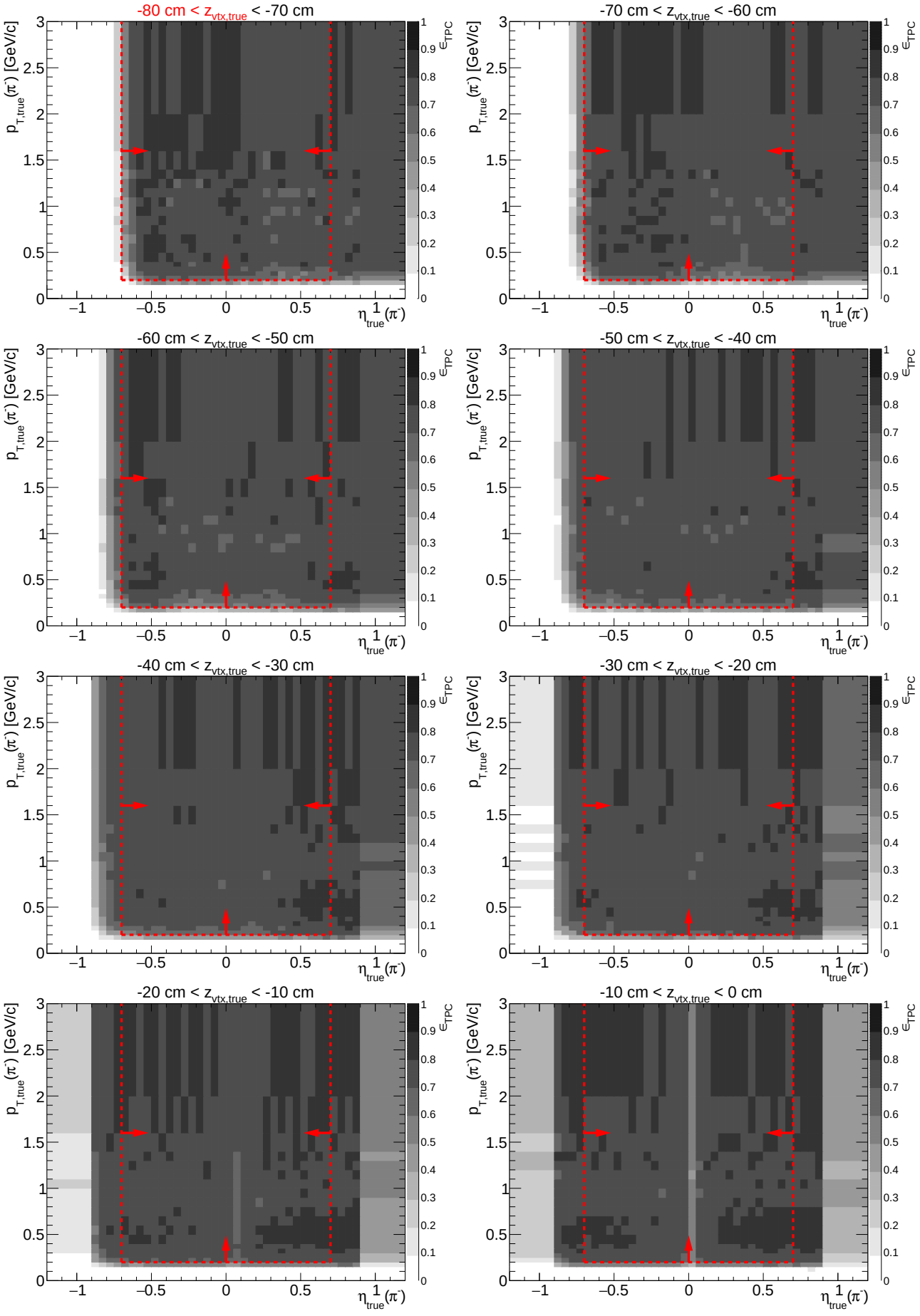

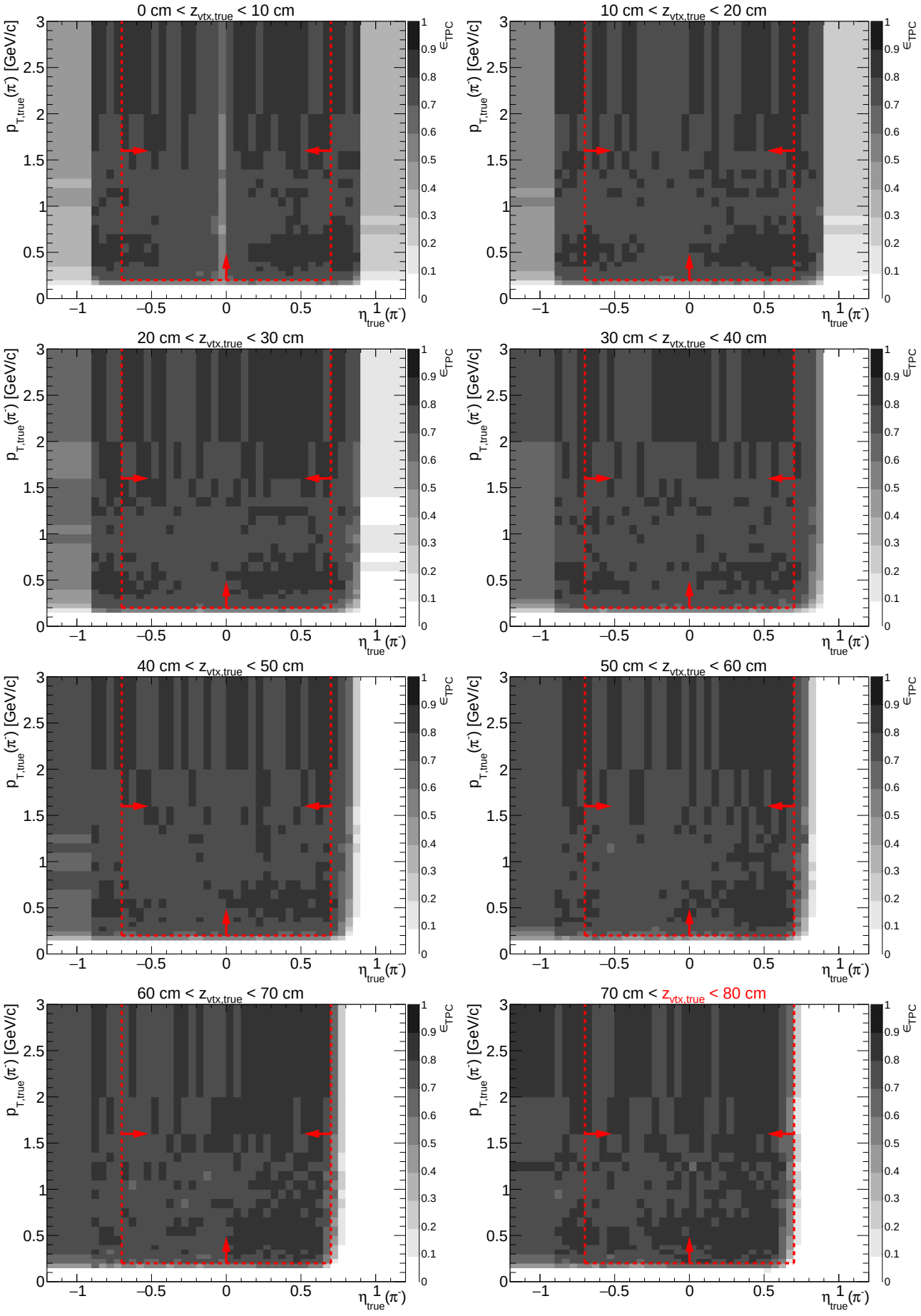
0 cm < z_vtx,true < 10 cm
10 cm < z_vtx,true < 20 cm
20 cm < z_vtx,true < 30 cm
30 cm < z_vtx,true < 40 cm
40 cm < z_vtx,true < 50 cm
50 cm < z_vtx,true < 60 cm
60 cm < z_vtx,true < 70 cm
70 cm < z_vtx,true < 80 cm
p_T,true(π⁻) [GeV/c]
η_true(π⁻)
ε_TPC

Figure 1.2: TPC acceptance and reconstruction efficiency of $\pi^+$. Each plot represents the TPC efficiency $\epsilon_{\mathrm{TPC}}$ ($z$-axis) as a function of true particle pseudorapidity $\eta$ ($x$-axis) and transverse momentum $p_T$ ($y$-axis) in single $z$-vertex bin whose range is given at the top. Red lines and arrows indicate region accepted in analyses.

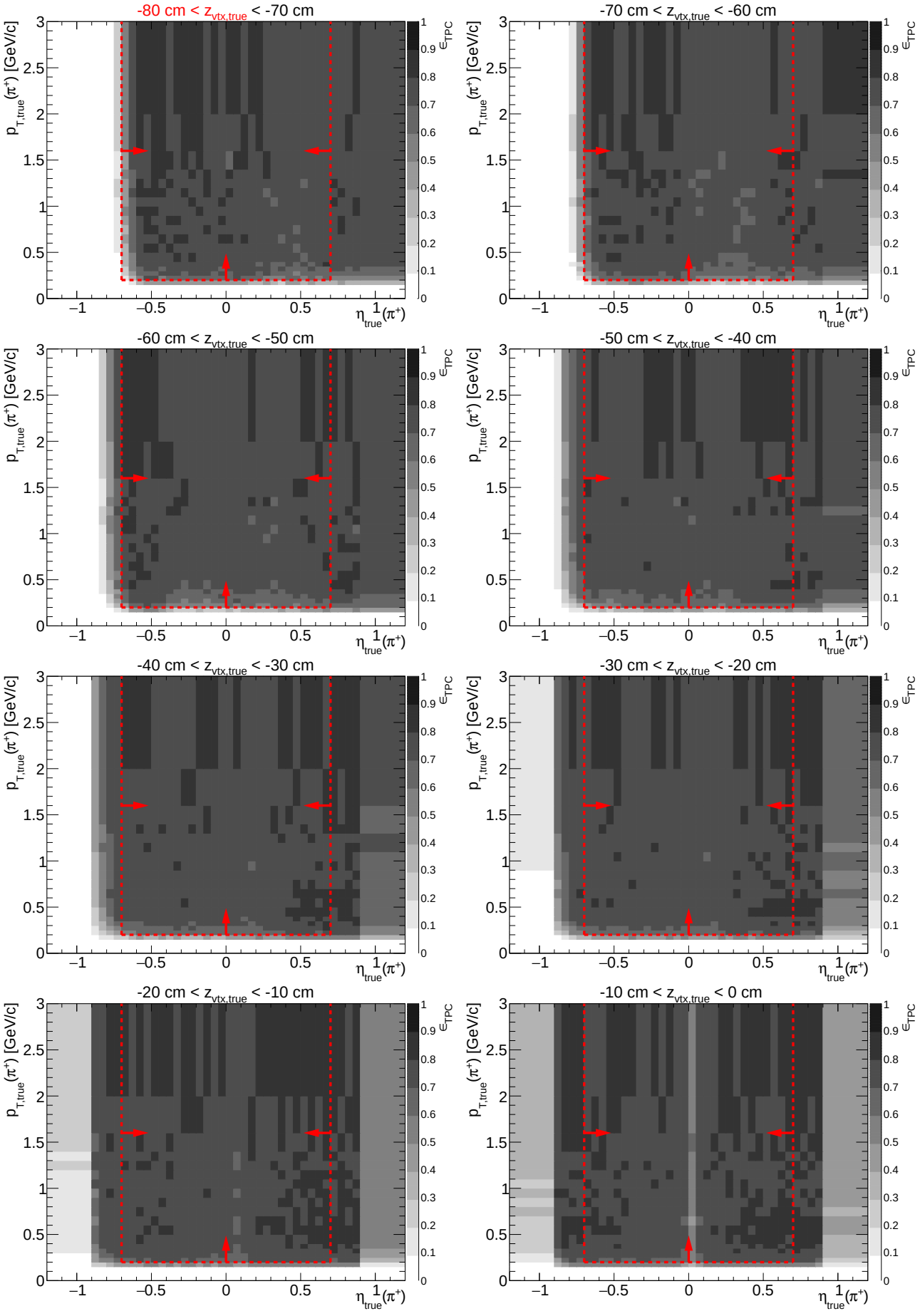

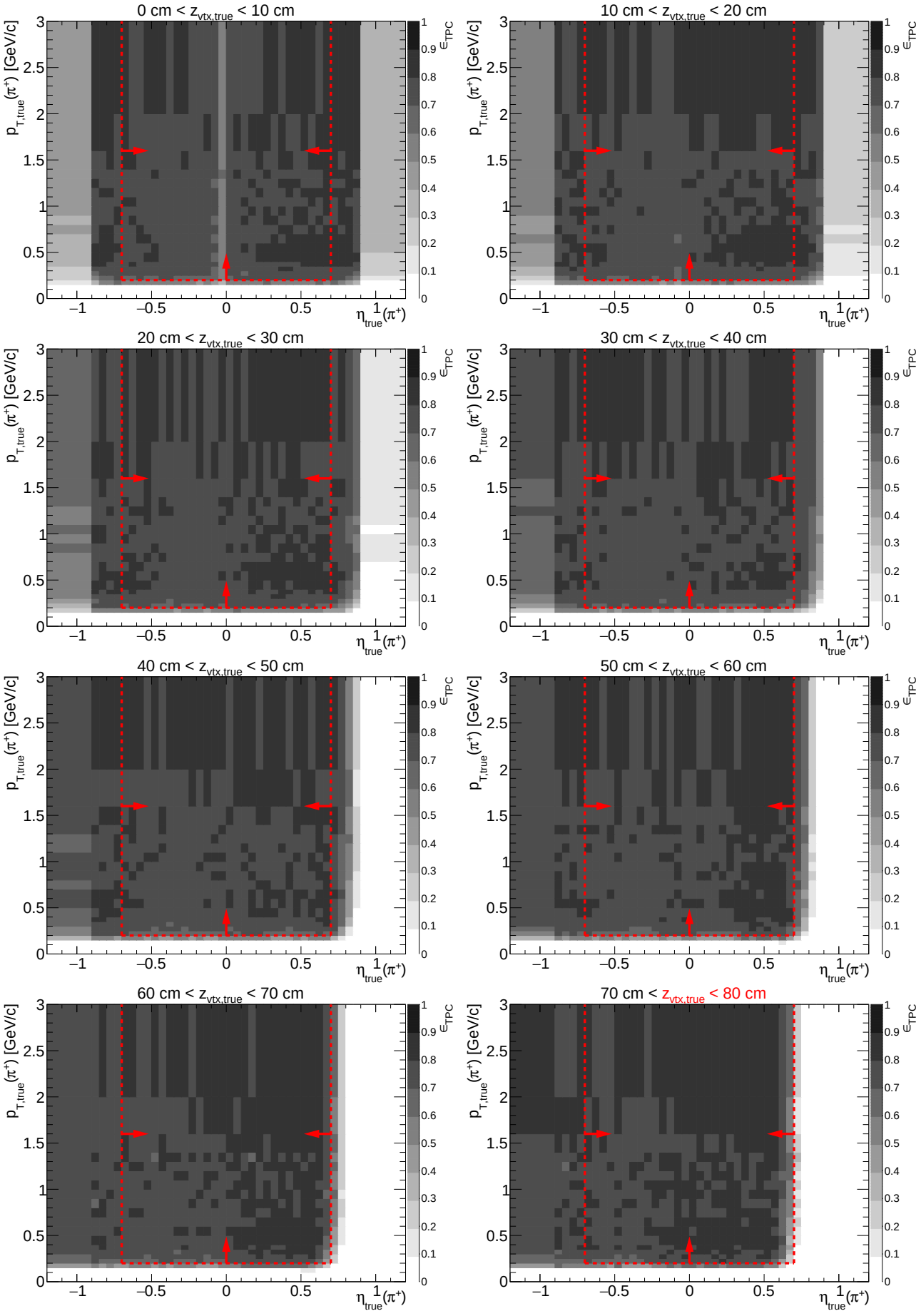
0 cm < z_vtx,true < 10 cm
10 cm < z_vtx,true < 20 cm
20 cm < z_vtx,true < 30 cm
30 cm < z_vtx,true < 40 cm
40 cm < z_vtx,true < 50 cm
50 cm < z_vtx,true < 60 cm
60 cm < z_vtx,true < 70 cm
70 cm < z_vtx,true < 80 cm
p_T,true(π+) [GeV/c]
η_true(π+)
ε_TPC

Figure 1.3: TPC acceptance and reconstruction efficiency of $K^-$. Each plot represents the TPC efficiency $\epsilon_{\mathrm{TPC}}$ ($z$-axis) as a function of true particle pseudorapidity $\eta$ ($x$-axis) and transverse momentum $p_T$ ($y$-axis) in single $z$-vertex bin whose range is given at the top. Red lines and arrows indicate region accepted in analyses.

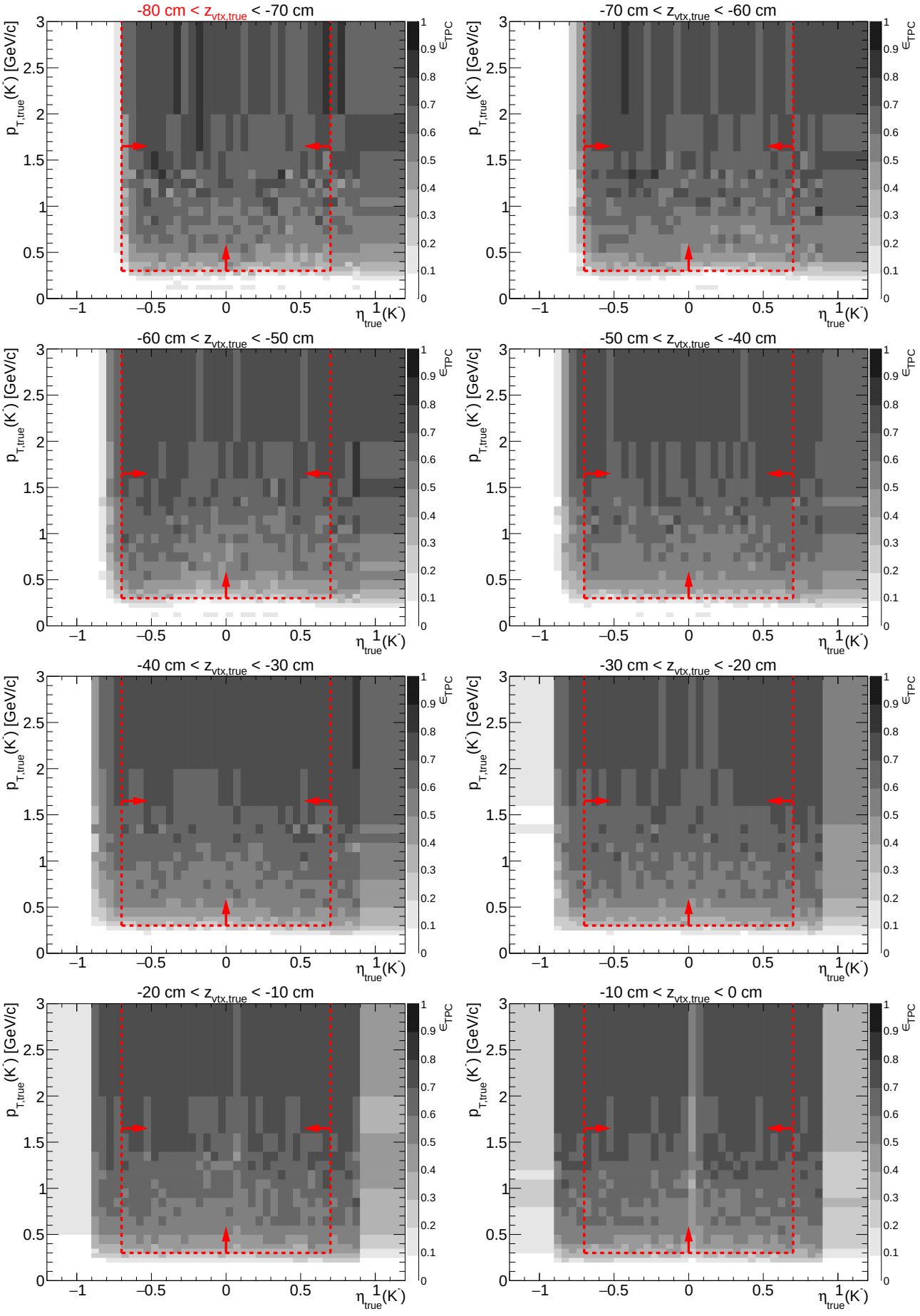

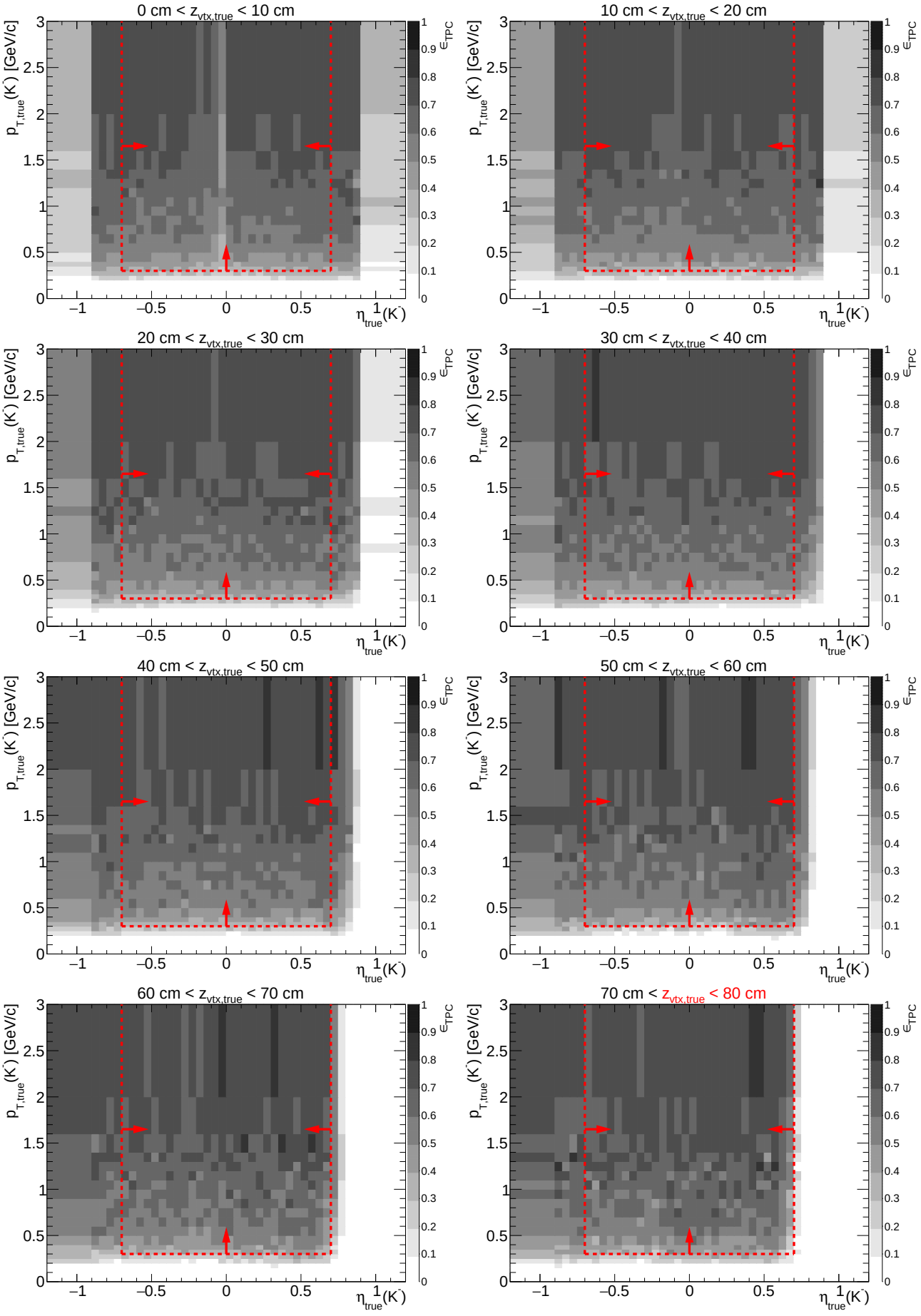
0 cm < z_vtx,true < 10 cm
10 cm < z_vtx,true < 20 cm
20 cm < z_vtx,true < 30 cm
30 cm < z_vtx,true < 40 cm
40 cm < z_vtx,true < 50 cm
50 cm < z_vtx,true < 60 cm
60 cm < z_vtx,true < 70 cm
70 cm < z_vtx,true < 80 cm
p_T,true(K⁻) [GeV/c]
η_true(K⁻)
ε_TPC

Figure 1.4: TPC acceptance and reconstruction efficiency of $K^+$. Each plot represents the TPC efficiency $\epsilon_{\mathrm{TPC}}$ ($z$-axis) as a function of true particle pseudorapidity $\eta$ ($x$-axis) and transverse momentum $p_T$ ($y$-axis) in single $z$-vertex bin whose range is given at the top. Red lines and arrows indicate region accepted in analyses.

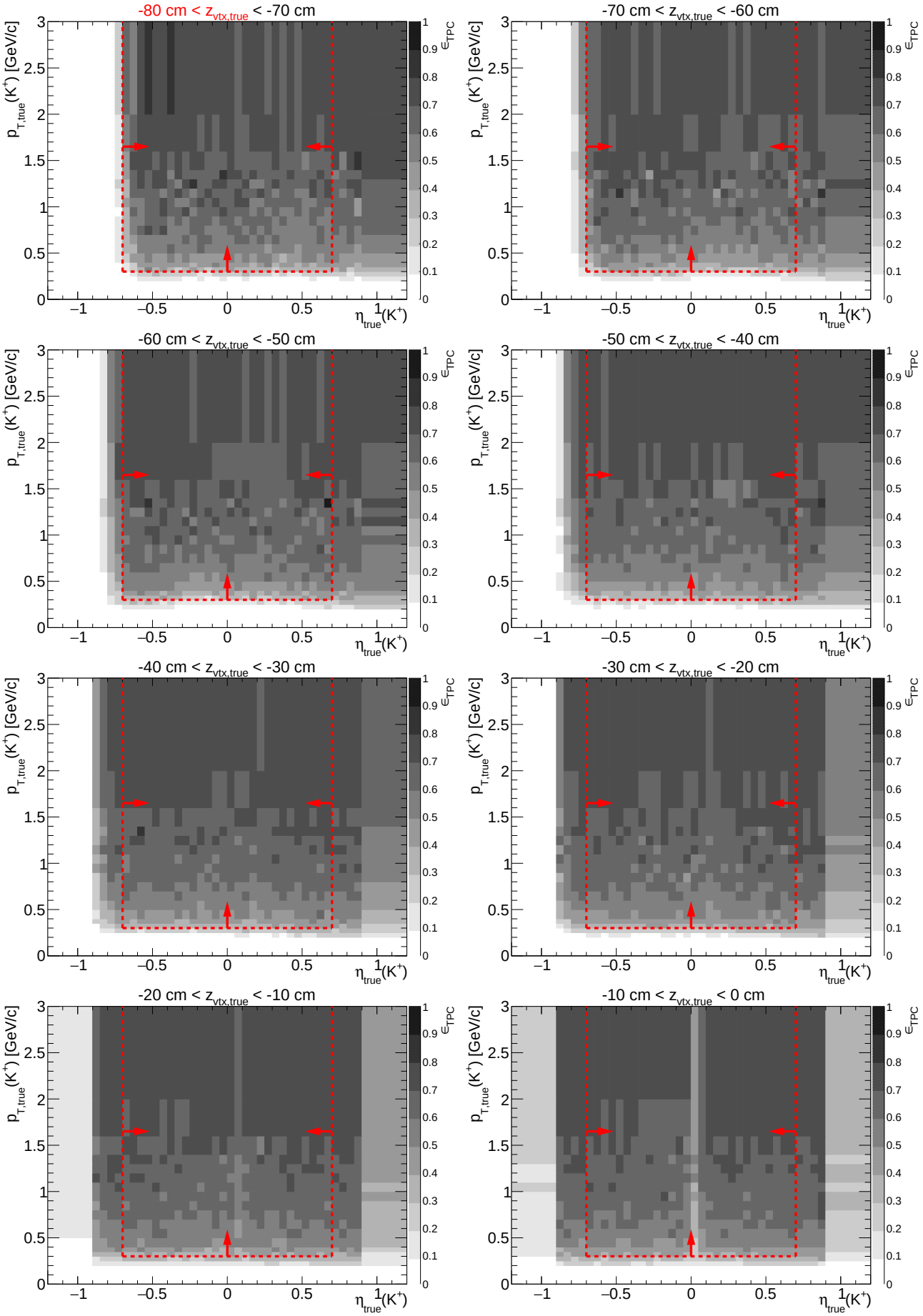

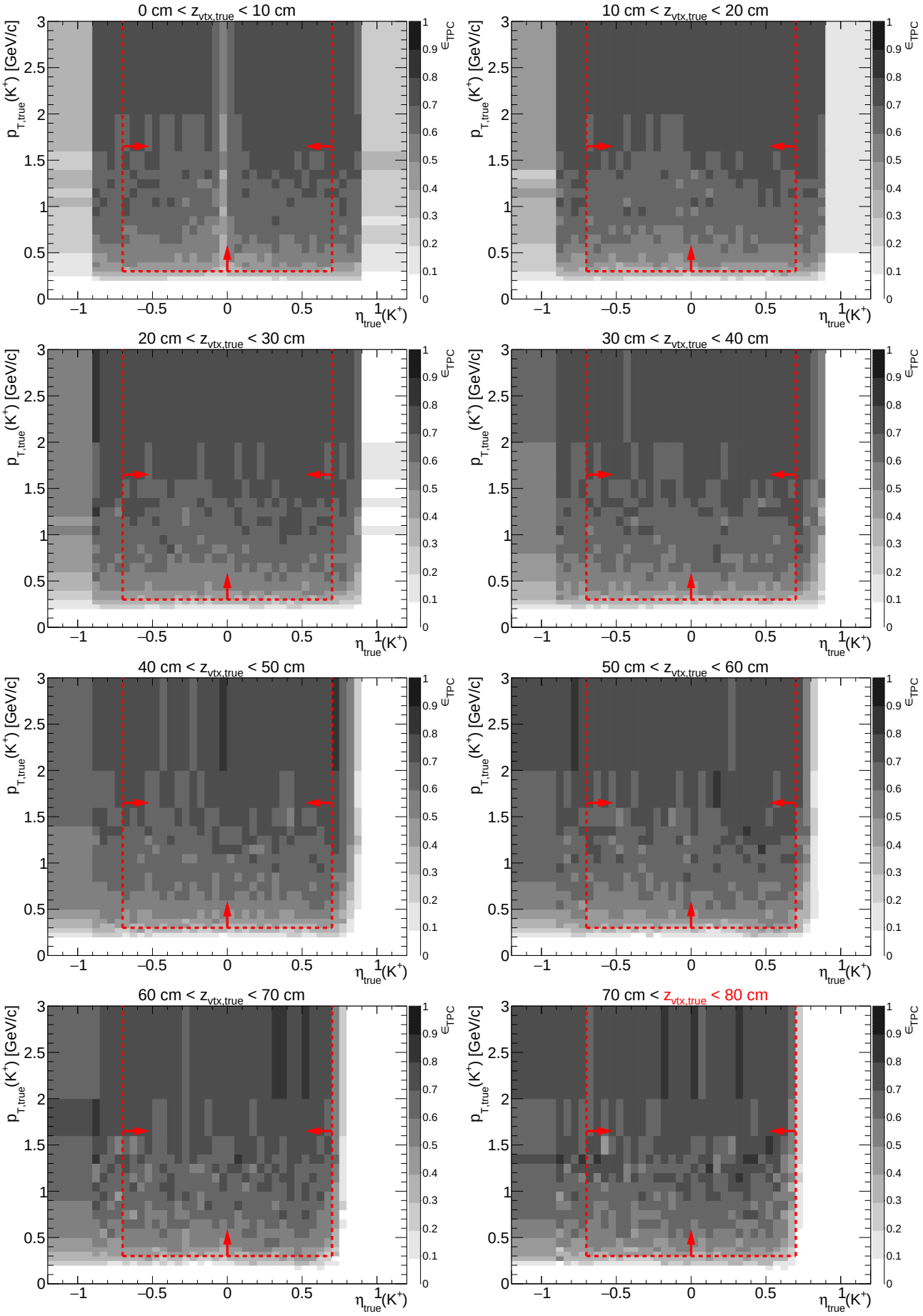
0 cm < z_vtx,true < 10 cm
10 cm < z_vtx,true < 20 cm
20 cm < z_vtx,true < 30 cm
30 cm < z_vtx,true < 40 cm
40 cm < z_vtx,true < 50 cm
50 cm < z_vtx,true < 60 cm
60 cm < z_vtx,true < 70 cm
70 cm < z_vtx,true < 80 cm
p_T,true (K+) [GeV/c]
η_true (K+)
ε_TPC

Figure 1.5: TPC acceptance and reconstruction efficiency of $\bar{p}$. Each plot represents the TPC efficiency $\epsilon_{\mathrm{TPC}}$ ($z$-axis) as a function of true particle pseudorapidity $\eta$ ($x$-axis) and transverse momentum $p_T$ ($y$-axis) in single $z$-vertex bin whose range is given at the top. Red lines and arrows indicate region accepted in analyses.

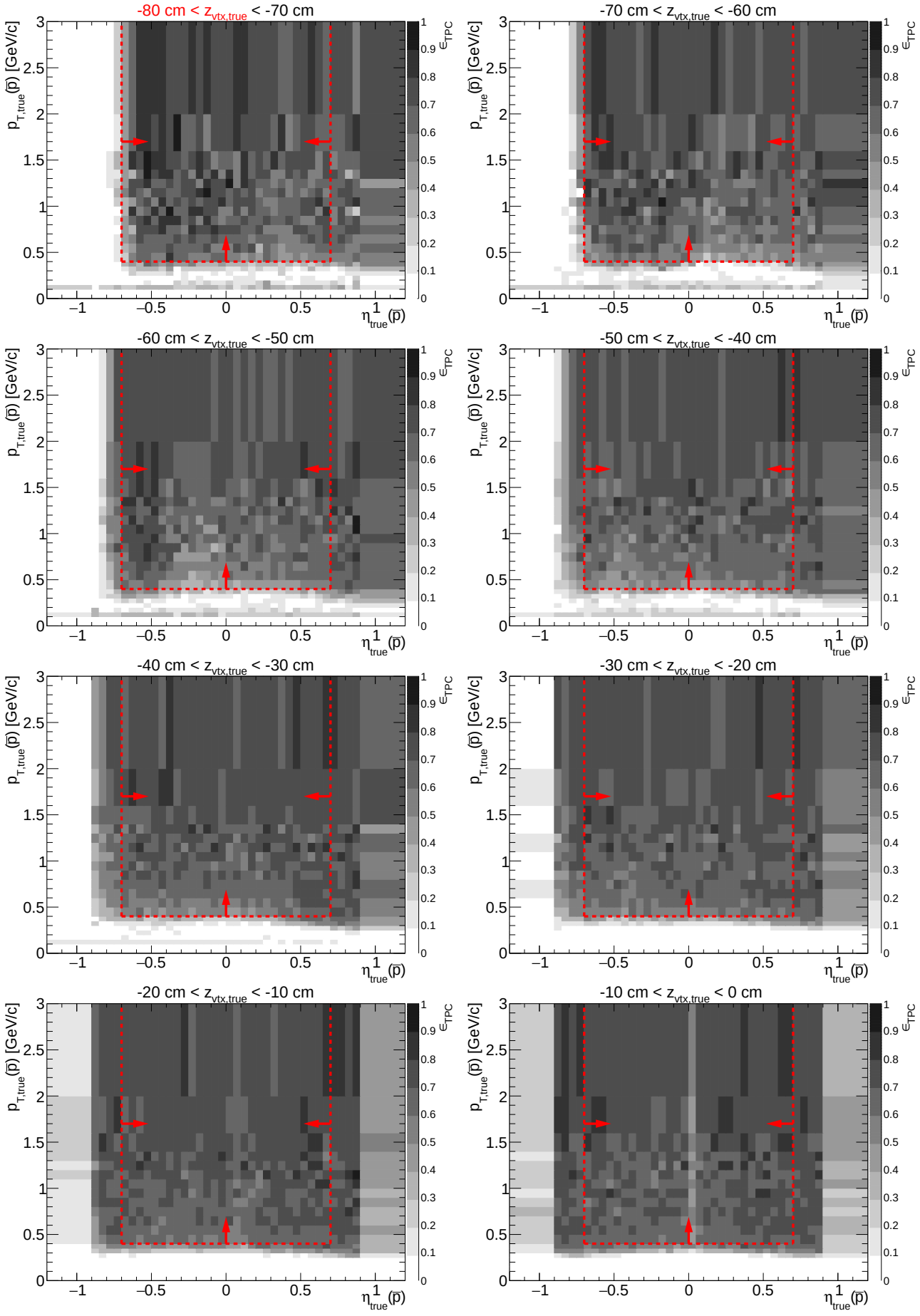

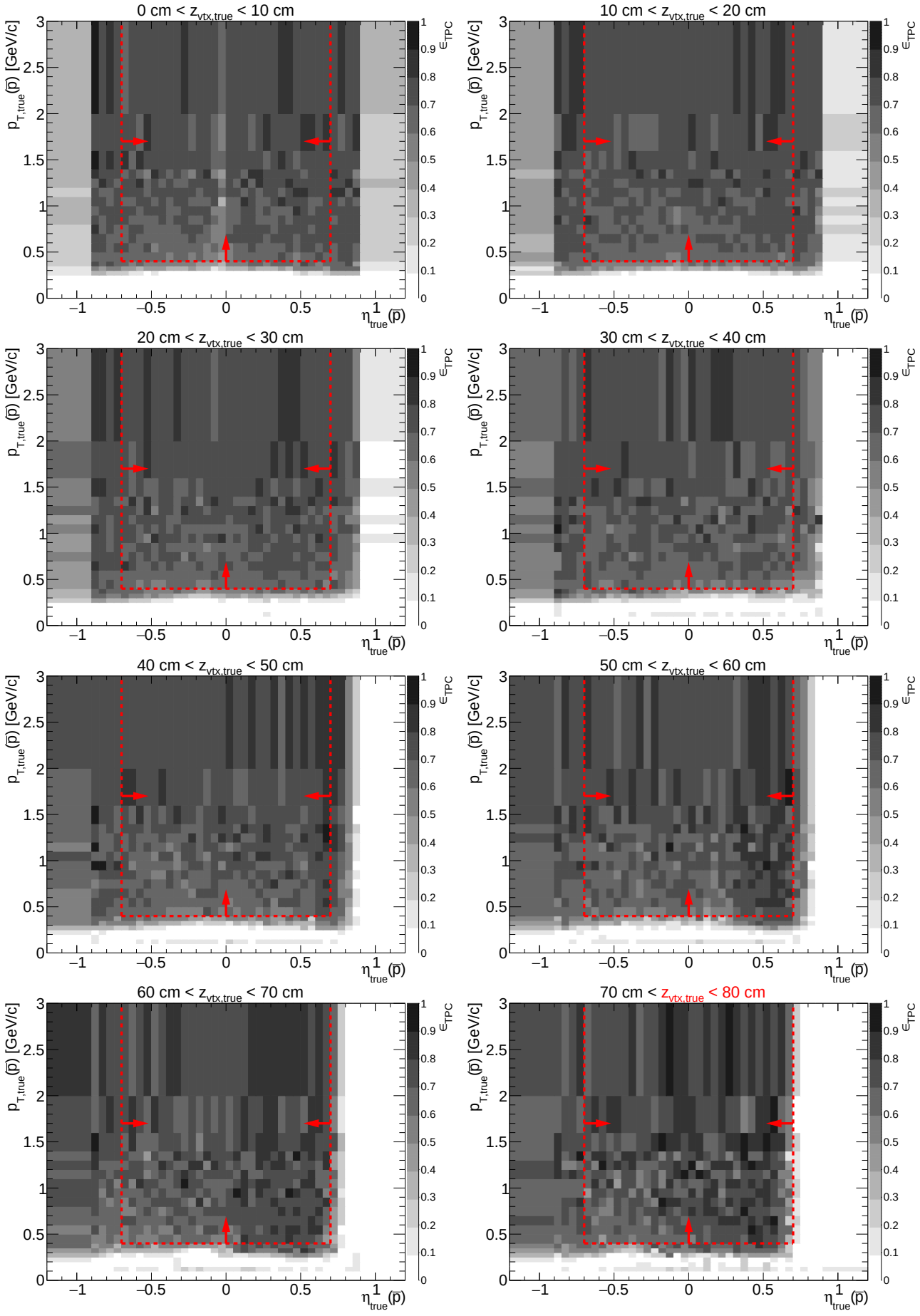
0 cm < z_vtx,true < 10 cm
10 cm < z_vtx,true < 20 cm
20 cm < z_vtx,true < 30 cm
30 cm < z_vtx,true < 40 cm
40 cm < z_vtx,true < 50 cm
50 cm < z_vtx,true < 60 cm
60 cm < z_vtx,true < 70 cm
70 cm < z_vtx,true < 80 cm
p_T,true(p̄) [GeV/c]
η_true(p̄)
ε_TPC

Figure 1.6: TPC acceptance and reconstruction efficiency of $p$. Each plot represents the TPC efficiency $\epsilon_{\mathrm{TPC}}$ ($z$-axis) as a function of true particle pseudorapidity $\eta$ ($x$-axis) and transverse momentum $p_T$ ($y$-axis) in single $z$-vertex bin whose range is given at the top. Red lines and arrows indicate region accepted in analyses.

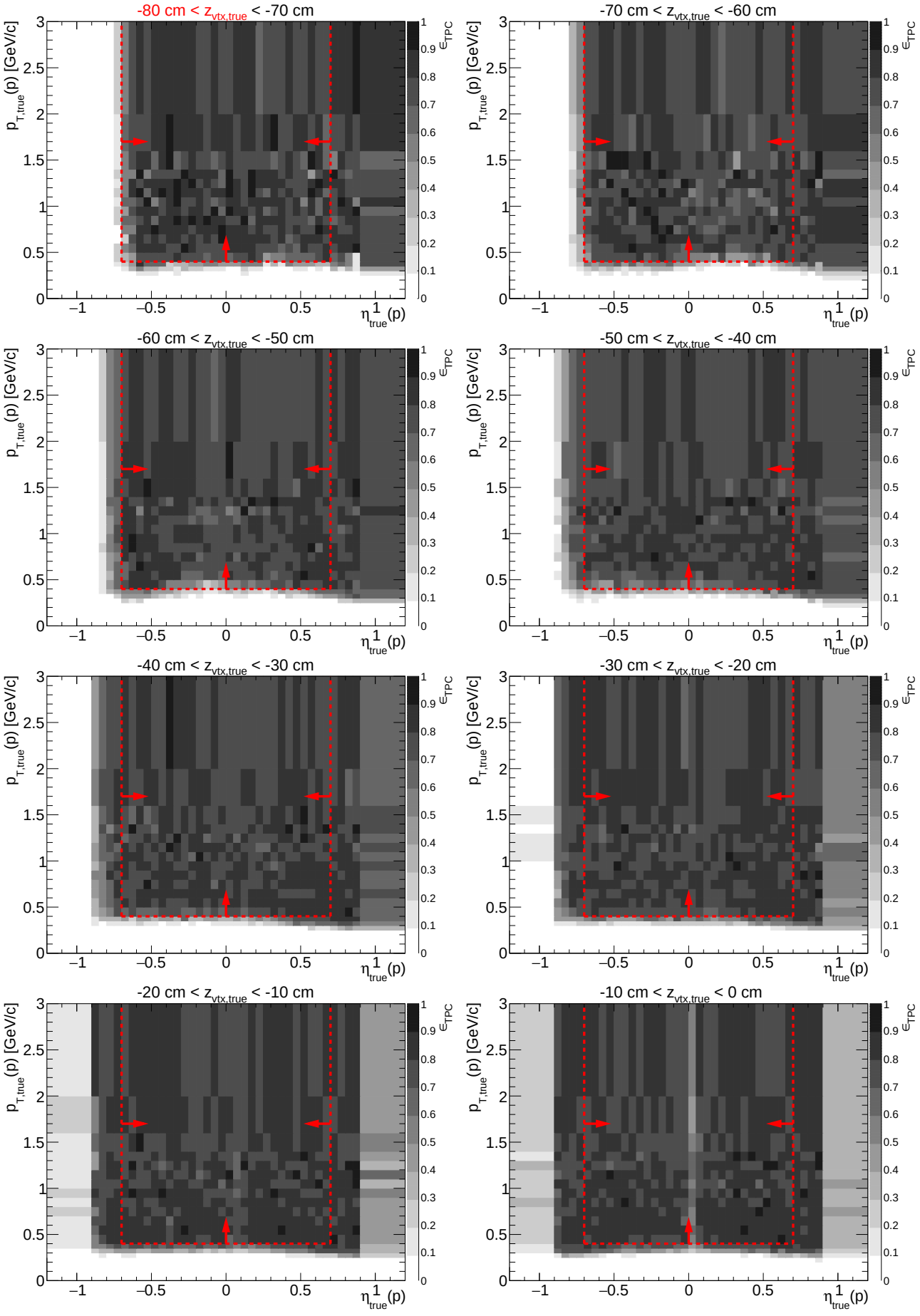

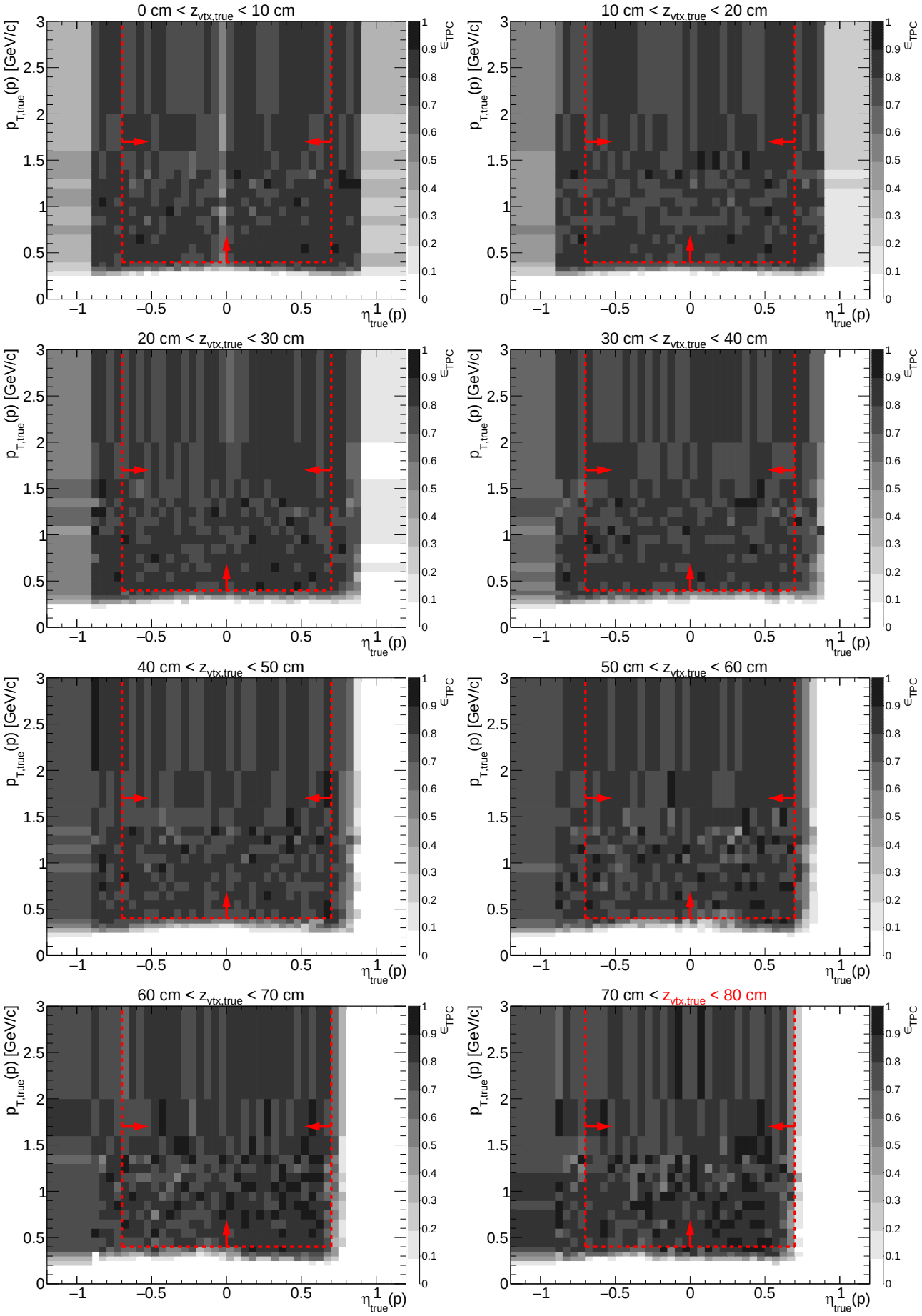
0 cm < z_vtx,true < 10 cm
10 cm < z_vtx,true < 20 cm
20 cm < z_vtx,true < 30 cm
30 cm < z_vtx,true < 40 cm
40 cm < z_vtx,true < 50 cm
50 cm < z_vtx,true < 60 cm
60 cm < z_vtx,true < 70 cm
70 cm < z_vtx,true < 80 cm
p_T,true (p) [GeV/c]
η_true (p)
ε_TPC

## 1.2 TOF acceptance, hit reconstruction and track-matching efficiency

Combined TOF acceptance, hit reconstruction efficiency and matching efficiency with TPC tracks, $\epsilon_{\mathrm{TOF}}$, is defined as the probability that the global TPC track that satisfy kinematic and quality criteria (cuts **??** and **??**) is matched with hit in TOF (matching flag of the track is different from 0). This quantity is generally referred as "TOF efficiency".

It is calculated in two ways. In the first approach the STARsim MC embedded into zero-bias triggers is used. Tracks belonging to *set B* from Sec. **??** are utilized. From these tracks a sub-sample of tracks with non-zero TOF matching flag is extracted (*set C*). The TOF efficiency is calculated as

$$\epsilon_{\mathrm{TOF}}\left(p_T, \eta, z_{vx};\ \mathrm{sign}, \mathrm{PID}\right) = \frac{(p_T, \eta, z_{vx}) \text{ histogram for particles of given sign and ID from } \textit{set } C}{(p_T, \eta, z_{vx}) \text{ histogram for particles of given sign and ID from } \textit{set } B}. \tag{1.2}$$

Figure 1.7: TOF acceptance, reconstruction and matching efficiency of $\pi^-$. Each plot represents the TOF efficiency $\epsilon_{\mathrm{TOF}}$ ($z$-axis) as a function of true particle pseudorapidity $\eta$ ($x$-axis) and transverse momentum $p_T$ ($y$-axis) in single $z$-vertex bin whose range is given at the top. Red lines and arrows indicate region accepted in analyses.

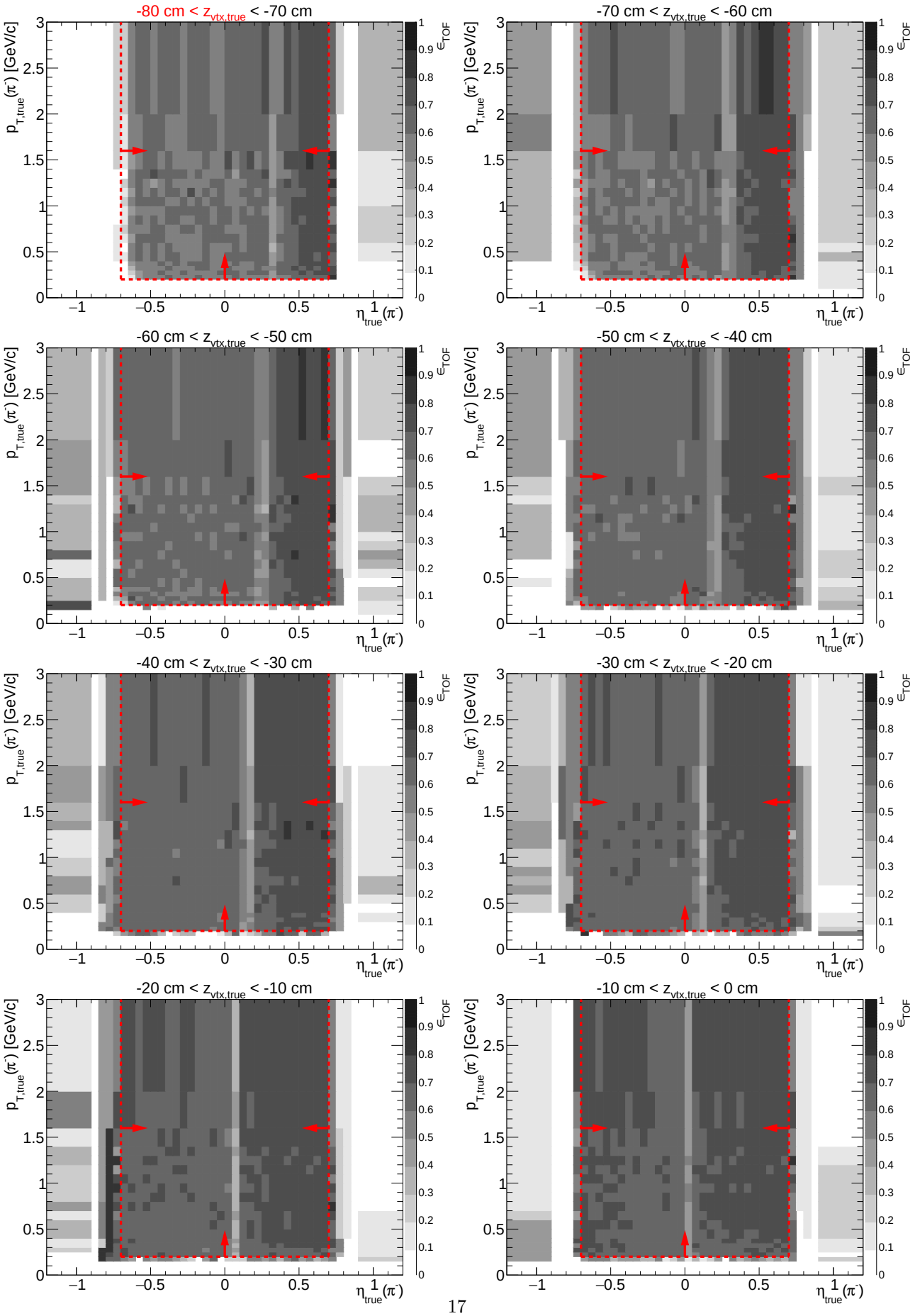

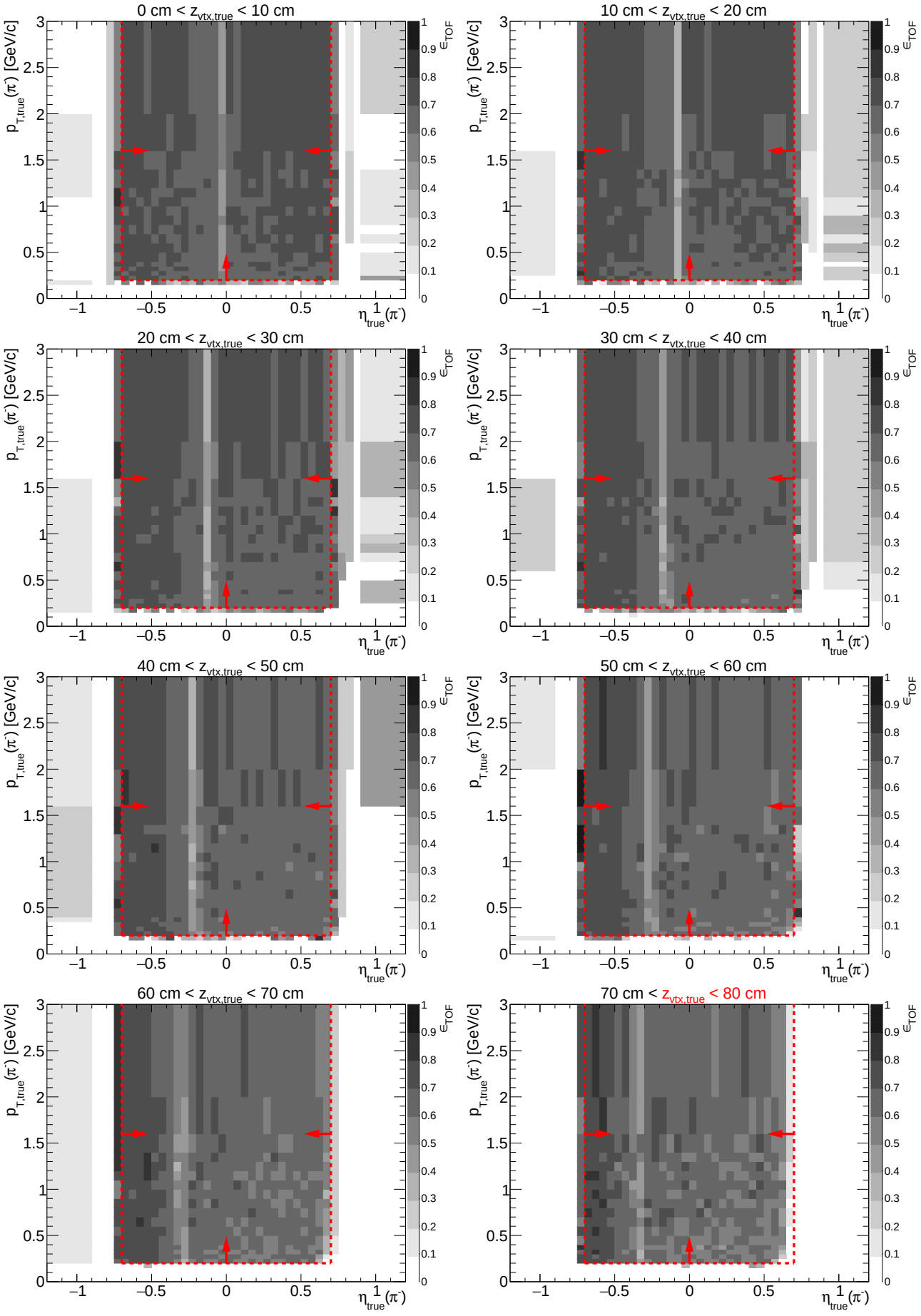
0 cm < z_vtx,true < 10 cm
10 cm < z_vtx,true < 20 cm
20 cm < z_vtx,true < 30 cm
30 cm < z_vtx,true < 40 cm
40 cm < z_vtx,true < 50 cm
50 cm < z_vtx,true < 60 cm
60 cm < z_vtx,true < 70 cm
70 cm < z_vtx,true < 80 cm
p_T,true (π⁻) [GeV/c]
η_true (π⁻)
ε_TOF

Figure 1.8: TOF acceptance, reconstruction and matching efficiency of $\pi^+$. Each plot represents the TOF efficiency $\epsilon_{\mathrm{TOF}}$ ($z$-axis) as a function of true particle pseudorapidity $\eta$ ($x$-axis) and transverse momentum $p_T$ ($y$-axis) in single $z$-vertex bin whose range is given at the top. Red lines and arrows indicate region accepted in analyses.

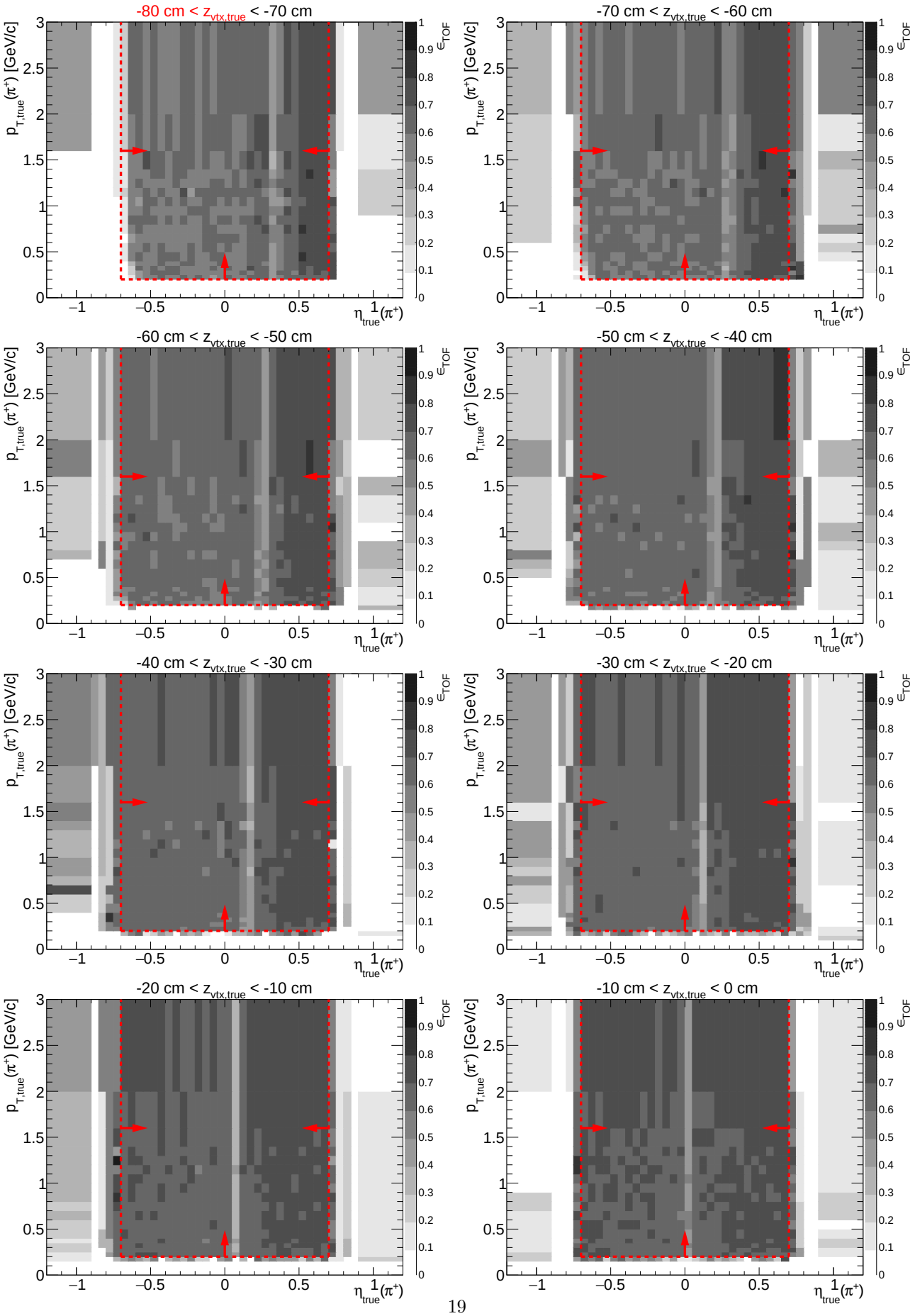

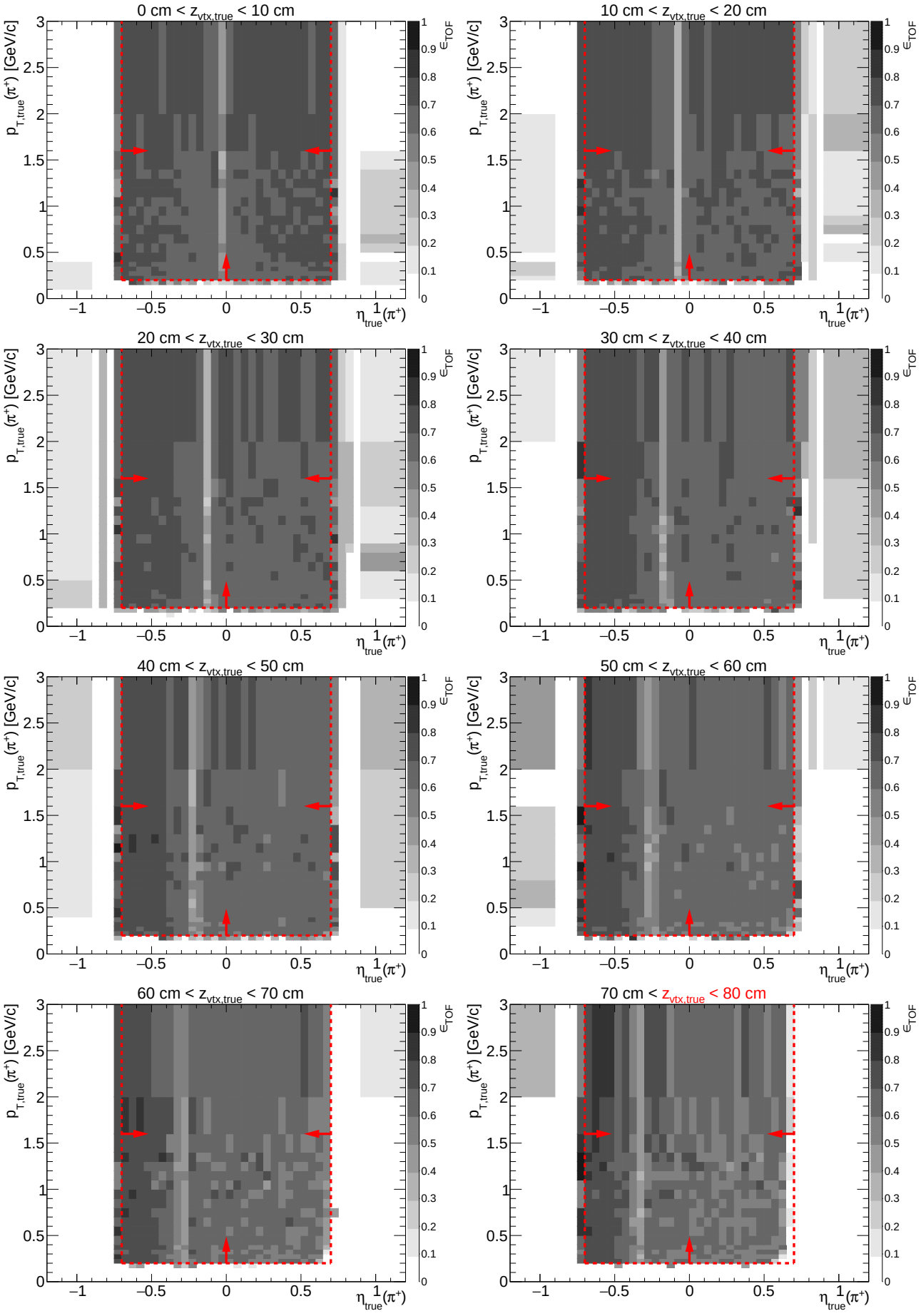
0 cm < z_vtx,true < 10 cm
10 cm < z_vtx,true < 20 cm
20 cm < z_vtx,true < 30 cm
30 cm < z_vtx,true < 40 cm
40 cm < z_vtx,true < 50 cm
50 cm < z_vtx,true < 60 cm
60 cm < z_vtx,true < 70 cm
70 cm < z_vtx,true < 80 cm
p_T,true (π+) [GeV/c]
η_true (π+)
ε_TOF

Figure 1.9: TOF acceptance, reconstruction and matching efficiency of $K^-$. Each plot represents the TOF efficiency $\epsilon_{\mathrm{TOF}}$ ($z$-axis) as a function of true particle pseudorapidity $\eta$ ($x$-axis) and transverse momentum $p_T$ ($y$-axis) in single $z$-vertex bin whose range is given at the top. Red lines and arrows indicate region accepted in analyses.

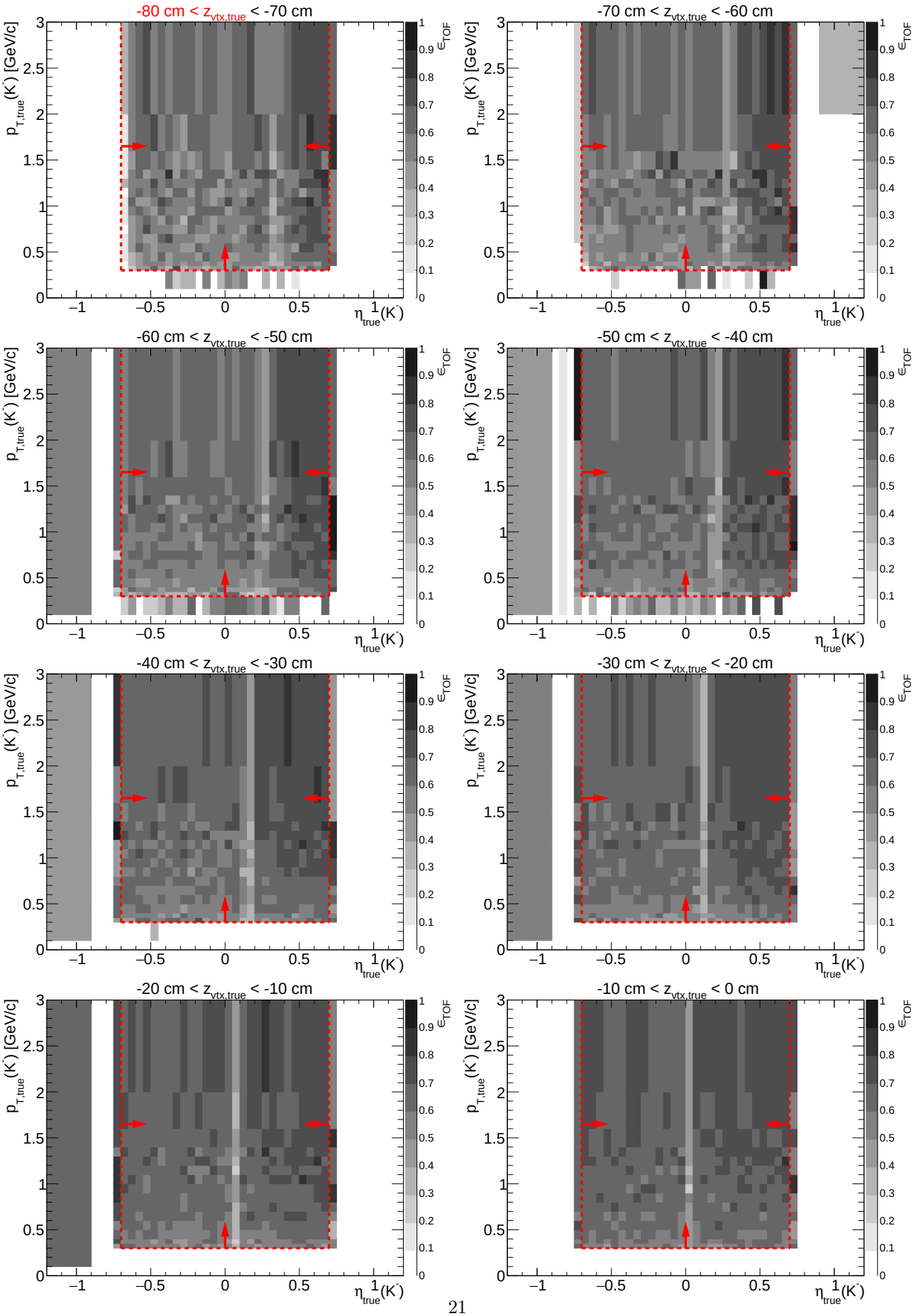

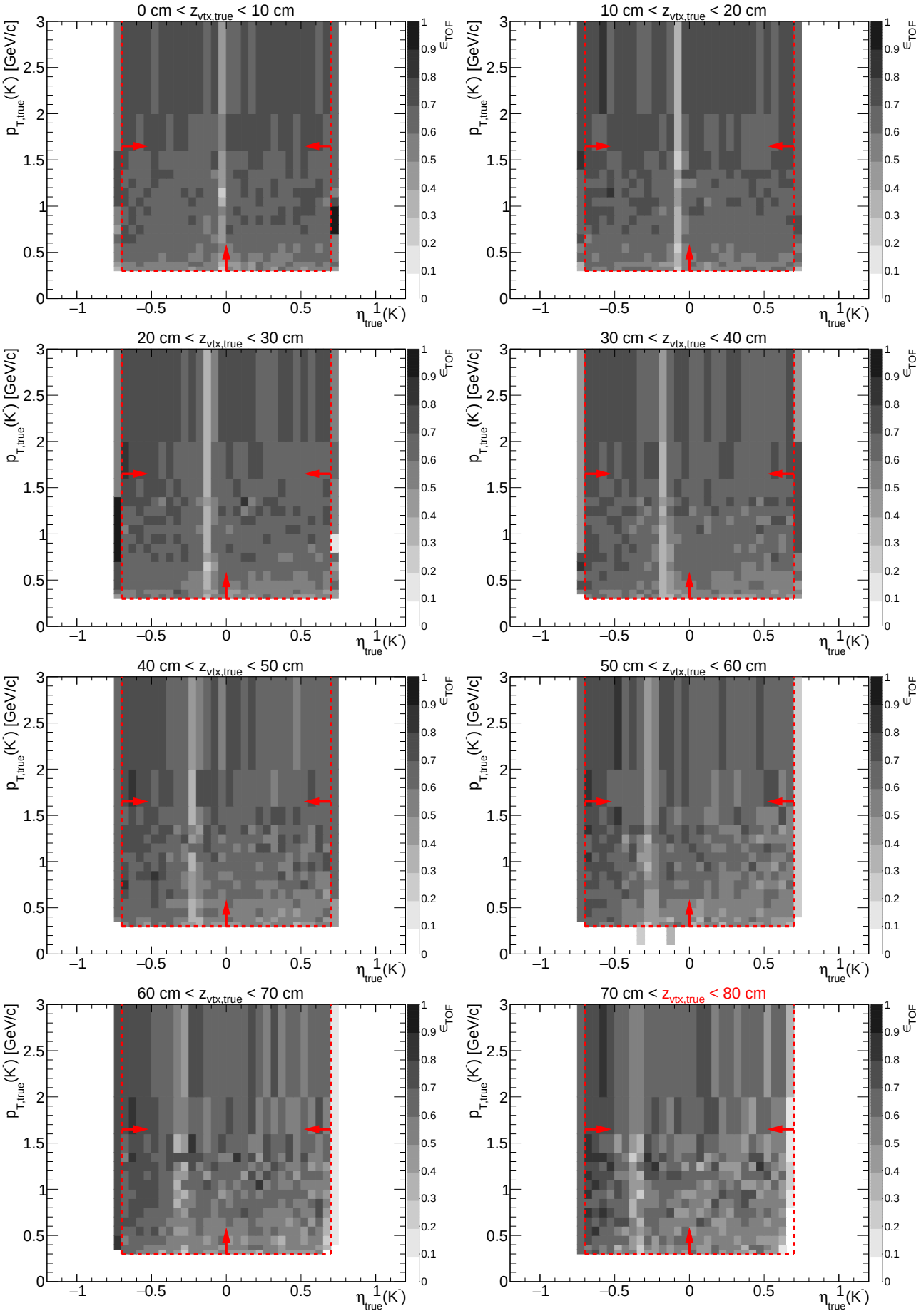
0 cm < z_vtx,true < 10 cm
10 cm < z_vtx,true < 20 cm
20 cm < z_vtx,true < 30 cm
30 cm < z_vtx,true < 40 cm
40 cm < z_vtx,true < 50 cm
50 cm < z_vtx,true < 60 cm
60 cm < z_vtx,true < 70 cm
70 cm < z_vtx,true < 80 cm
p_T,true(K⁻) [GeV/c]
η_true(K⁻)
ε_TOF

Figure 1.10: TOF acceptance, reconstruction and matching efficiency of $K^+$. Each plot represents the TOF efficiency $\epsilon_{\mathrm{TOF}}$ ($z$-axis) as a function of true particle pseudorapidity $\eta$ ($x$-axis) and transverse momentum $p_T$ ($y$-axis) in single $z$-vertex bin whose range is given at the top. Red lines and arrows indicate region accepted in analyses.

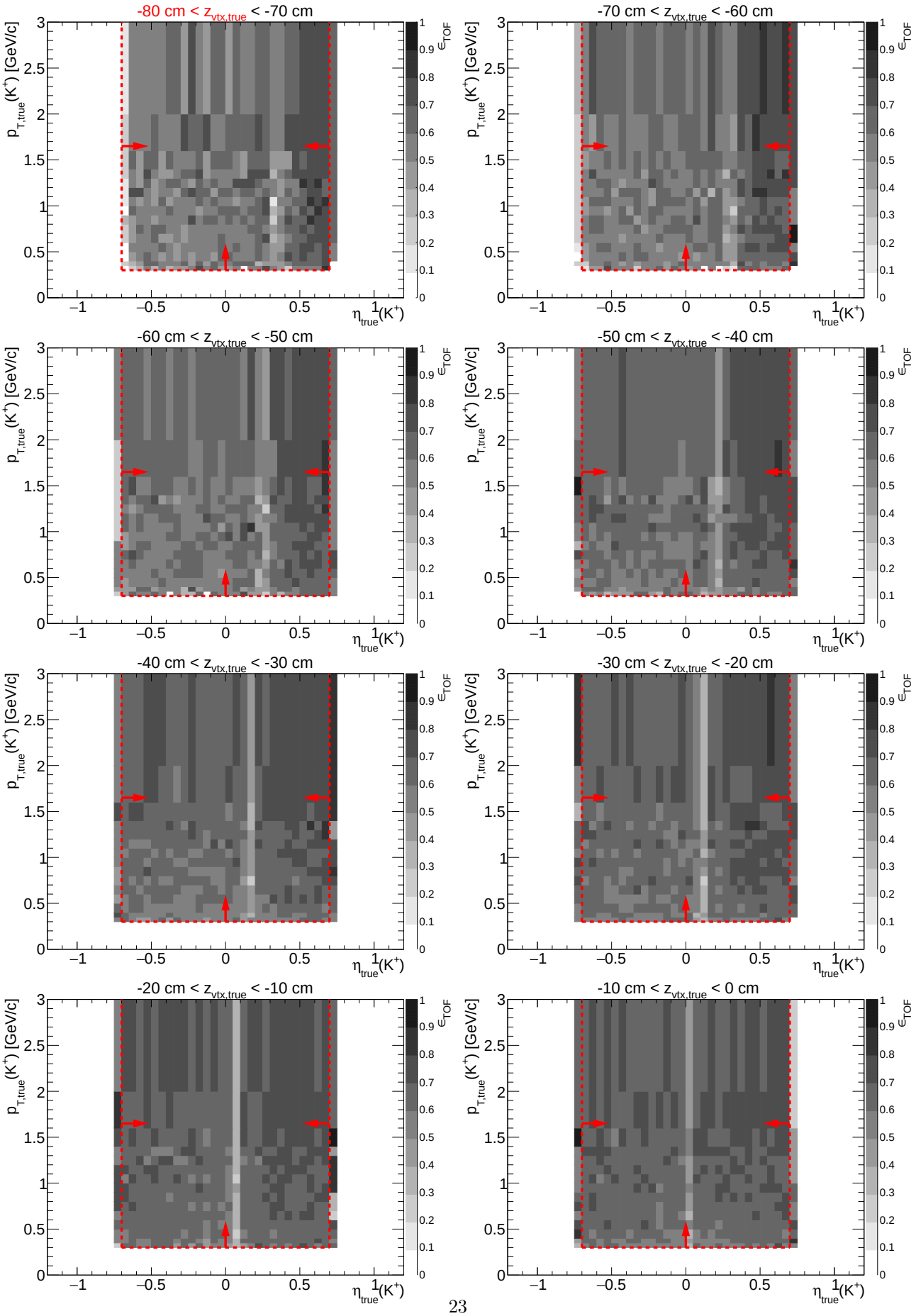

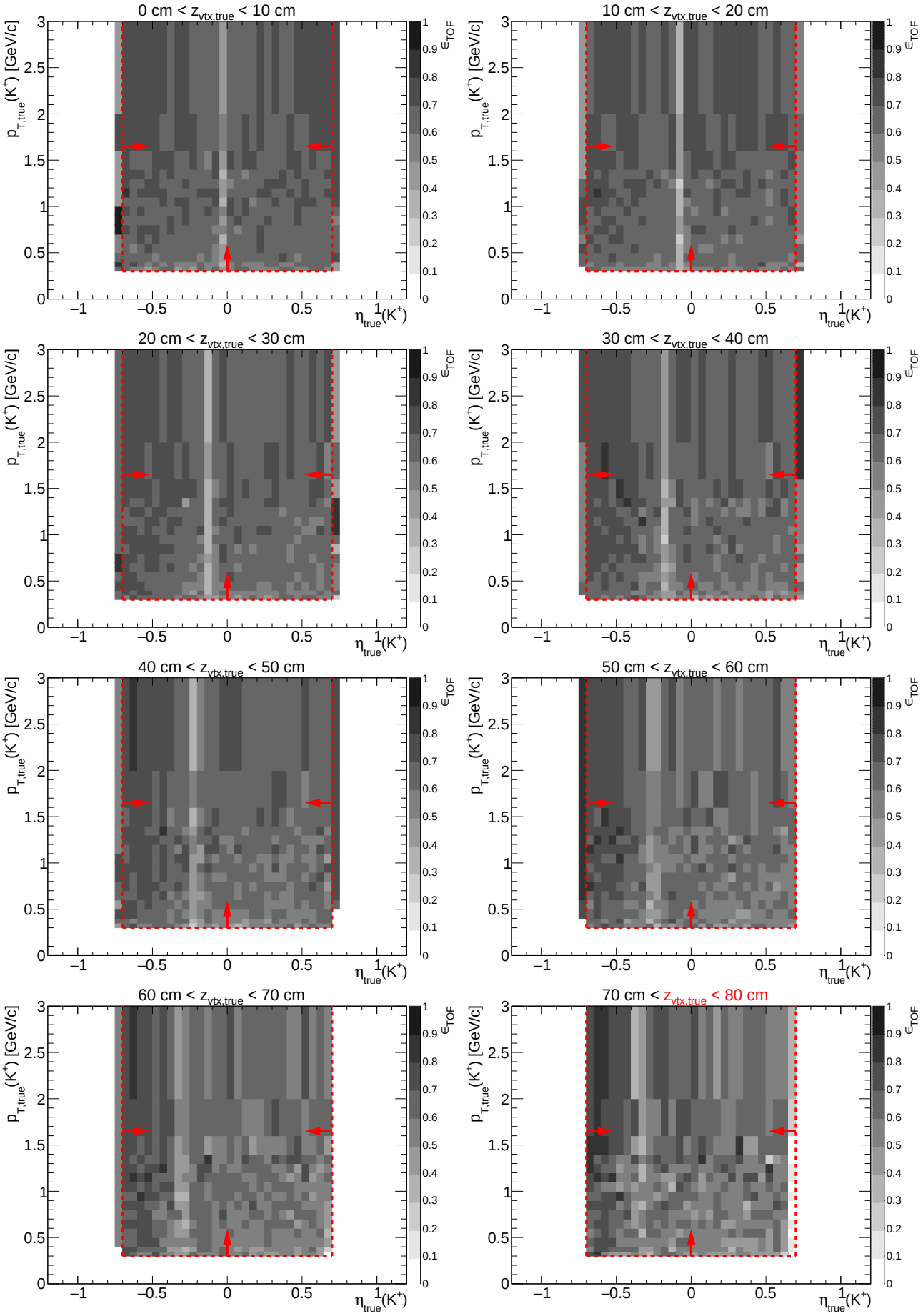
0 cm < z_vtx,true < 10 cm
10 cm < z_vtx,true < 20 cm
20 cm < z_vtx,true < 30 cm
30 cm < z_vtx,true < 40 cm
40 cm < z_vtx,true < 50 cm
50 cm < z_vtx,true < 60 cm
60 cm < z_vtx,true < 70 cm
70 cm < z_vtx,true < 80 cm
p_T,true (K+) [GeV/c]
η_true (K+)
ε_TOF

Figure 1.11: TOF acceptance, reconstruction and matching efficiency of $\bar{p}$. Each plot represents the TOF efficiency $\epsilon_{\mathrm{TOF}}$ ($z$-axis) as a function of true particle pseudorapidity $\eta$ ($x$-axis) and transverse momentum $p_T$ ($y$-axis) in single $z$-vertex bin whose range is given at the top. Red lines and arrows indicate region accepted in analyses.

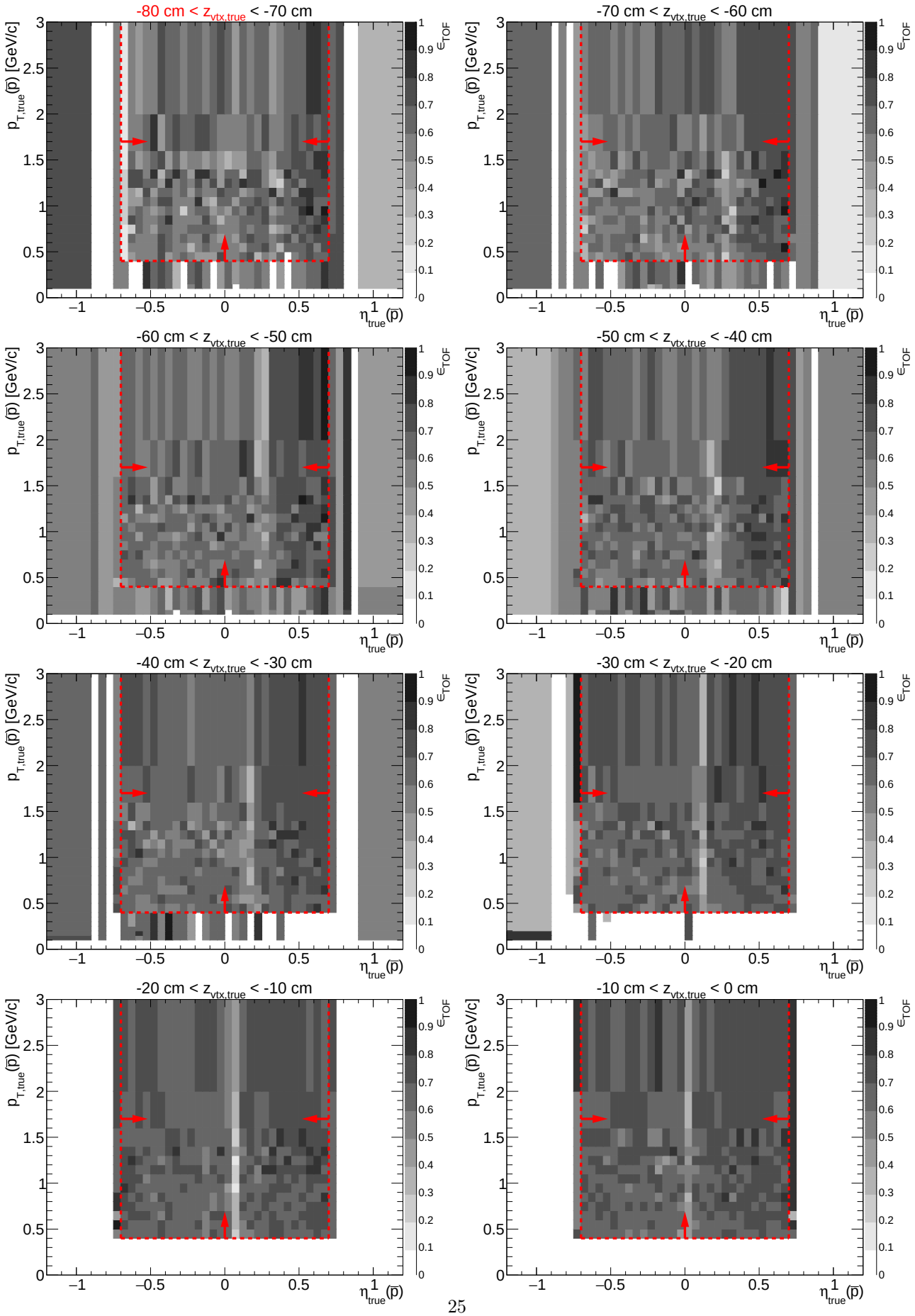

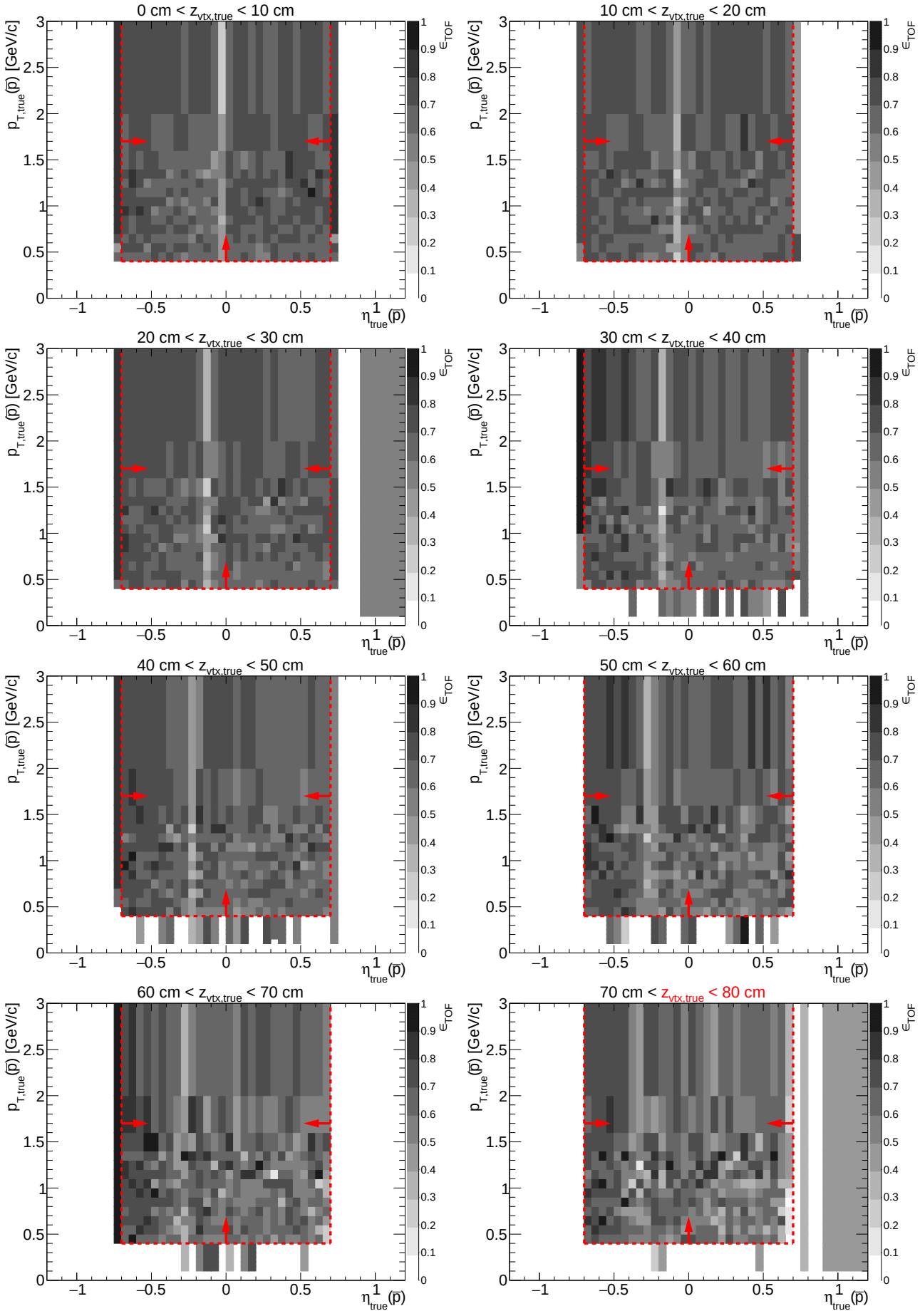
0 cm < z_vtx,true < 10 cm
10 cm < z_vtx,true < 20 cm
20 cm < z_vtx,true < 30 cm
30 cm < z_vtx,true < 40 cm
40 cm < z_vtx,true < 50 cm
50 cm < z_vtx,true < 60 cm
60 cm < z_vtx,true < 70 cm
70 cm < z_vtx,true < 80 cm
p_T,true(p̄) [GeV/c]
η_true(p̄)
ε_TOF

Figure 1.12: TOF acceptance, reconstruction and matching efficiency of $p$. Each plot represents the TOF efficiency $\epsilon_{\mathrm{TOF}}$ ($z$-axis) as a function of true particle pseudorapidity $\eta$ ($x$-axis) and transverse momentum $p_T$ ($y$-axis) in single $z$-vertex bin whose range is given at the top. Red lines and arrows indicate region accepted in analyses.

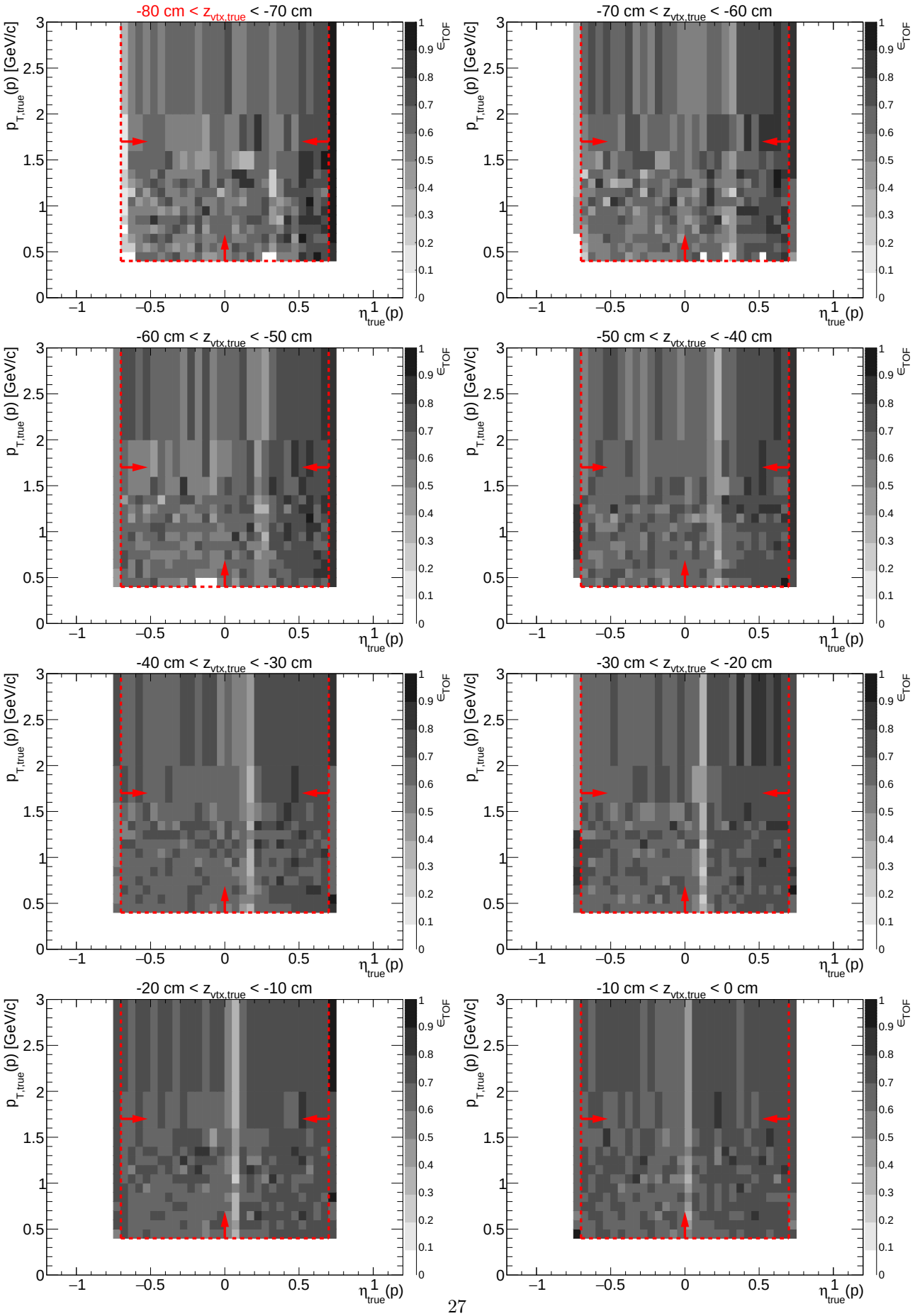

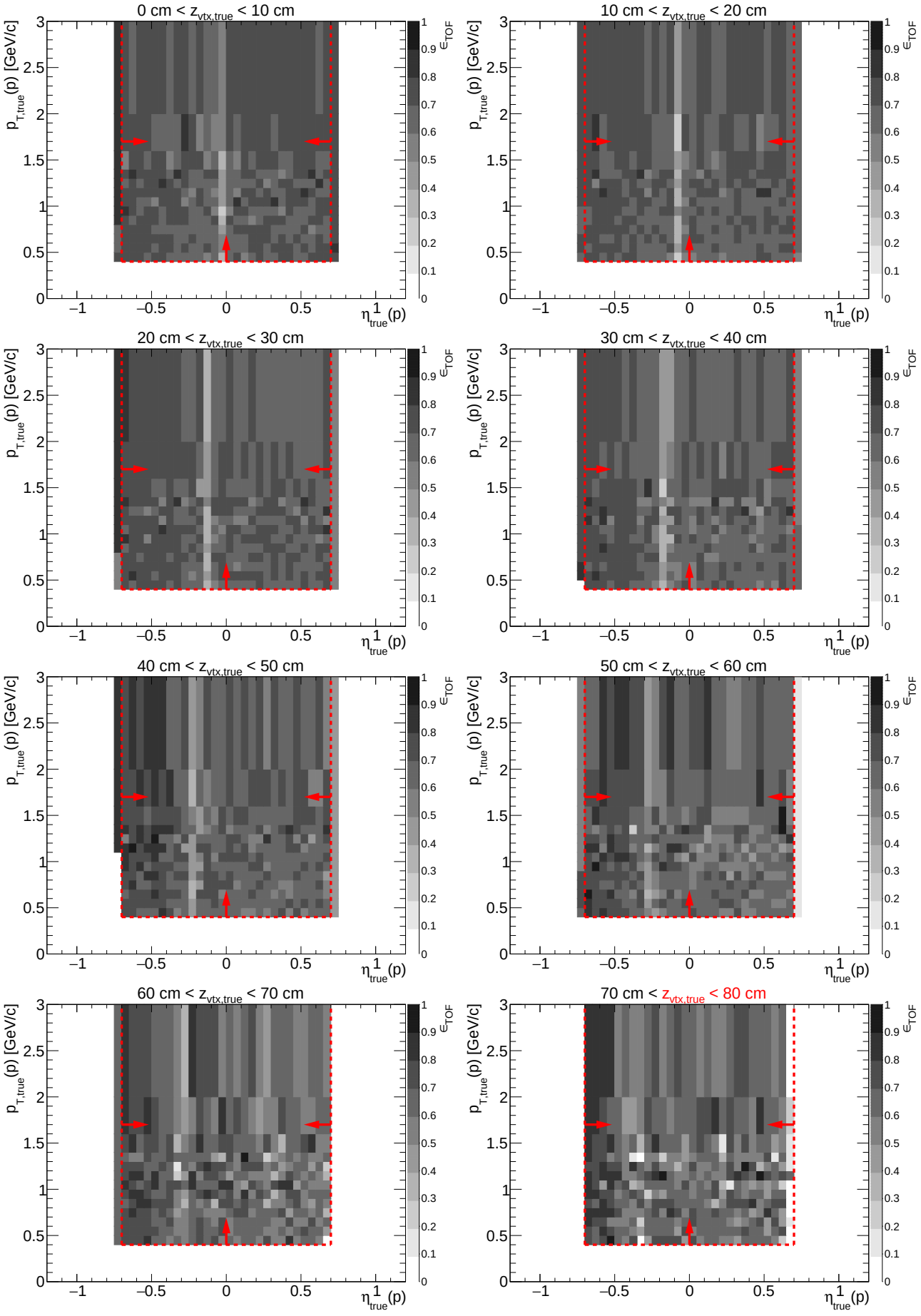
0 cm < z_vtx,true < 10 cm
10 cm < z_vtx,true < 20 cm
20 cm < z_vtx,true < 30 cm
30 cm < z_vtx,true < 40 cm
40 cm < z_vtx,true < 50 cm
50 cm < z_vtx,true < 60 cm
60 cm < z_vtx,true < 70 cm
70 cm < z_vtx,true < 80 cm
p_T,true (p) [GeV/c]
η_true (p)
ε_TOF

## 1.3 TPC vertex reconstruction efficiency

The definition of vertex reconstruction efficiency established in this analysis is the probability that two global tracks, both associated with true-level primary particles from the kinematic region of the measurement, both satisfying kinematic and quality criteria (cuts **??** and **??**) and both matched with hits in TOF, form a vertex listed in the collection of reconstructed primary vertices and DCA(R) and DCA(z) of both global tracks calculated w.r.t. this vertex is contained within the limits of cut **??**.

# 2. Roman Pot simulation

# 3. d$E/$d$x$ correction

It is possible to transform dE/dx in MC to make it follow the shape of dE/dx in the data. We know that nSigmaX (where X=Pion, Kaon, Proton, ...) variable follows a gaussian distribution (for particle X)

$$nSigmaX = \Big( \ln \frac{dE/dx}{\langle dE/dx \rangle_X} \Big) / \sigma_{dE/dx}, \qquad f(nSigmaX) = \mathcal{N}(nSigmaX; \mu = 0, \sigma = 1)$$

therefore $dE/dx$ itself follows log-normal distribution:

$$f(dE/dx) = \mathcal{L}og\mathcal{N}(dE/dx; \mu = \langle dE/dx \rangle, \sigma = \sigma_{dE/dx}) = \frac{1}{\sqrt{2\pi} \cdot \sigma \cdot dE/dx} e^{-\frac{\ln^2 \frac{dE/dx}{\langle dE/dx \rangle}}{2\sigma^2}}$$

The transformation we want to apply should preserve the shape of $dE/dx$ (so that it is still described by $\mathcal{L}og\mathcal{N}$), however it should change $\mu$ and $\sigma$ so that these values are euqal to those seen in the data. The transformation that satisfies above postulate is

$$dE/dx' = c \cdot (dE/dx)^a$$

Parameters of the distribution $\mathcal{L}og\mathcal{N}(dE/dx')$ would be then

$$\mu' = c \cdot \mu^a, \qquad \sigma' = a \cdot \sigma$$

From above we get formulae for parameters of the transformation:

$$a = \sigma'/\sigma, \qquad c = \frac{\mu'}{\mu^a}$$

AlternativeToCrystallBall [3] Eq. (3.1)

$$f(dE/dx) = \begin{cases} \frac{A}{\sqrt{2\pi} \cdot \sigma \cdot dE/dx} \exp\left( -\frac{1}{2} \left( \frac{\ln \frac{dE/dx}{\langle dE/dx \rangle}}{\sigma} \right)^2 \right) & \text{for } \frac{\ln \frac{dE/dx}{\langle dE/dx \rangle}}{\sigma} \leq k \\ \frac{A}{\sqrt{2\pi} \cdot \sigma \cdot dE/dx} \exp\left( -k \cdot \frac{\ln \frac{dE/dx}{\langle dE/dx \rangle}}{\sigma} + \frac{1}{2}k^2 - k^{-1} \left( \frac{\ln \frac{dE/dx}{\langle dE/dx \rangle}}{\frac{\sigma}{k}} - 1 \right)^k \right) & \text{for } \frac{\ln \frac{dE/dx}{\langle dE/dx \rangle}}{\sigma} > k \end{cases} \tag{3.1}$$

$$g(p) = P_1 + P_2 \cdot \exp\left(-P_3 \cdot p\right) + P_4 \cdot \arctan\left(P_5 \cdot (p - P_6)\right) \tag{3.2}$$

| PID | $\langle dE/dx\rangle_{\text{Bichsel}} - \langle dE/dx\rangle_{\text{MC}}$ | | | | | | $\sigma(dE/dx)_{\text{MC}}$ | | | | | |
|---|---|---|---|---|---|---|---|---|---|---|---|---|
| | $P_1$ | $P_2$ | $P_3$ | $P_4$ | $P_5$ | $P_6$ | $P_1$ | $P_2$ | $P_3$ | $P_4$ | $P_5$ | $P_6$ |
| $\pi^{\pm}$ | 3.618e-8 | 5.838e-9 | 5.481 | | | | 0.0809 | -0.023 | 0.450 | -7.84e-3 | 1.8489 | 1.04 |
| $K^{\pm}$ | -1.01e-10 | -9.983e-6 | 7.581 | | | | 0.0628 | 0.022 | 5.381 | 3.06e-3 | 7.3070 | 0.547 |
| $p, \bar{p}$ | -4.041e-8 | -1.179e-5 | 4.277 | | | | 0.0660 | 0.082 | 12.042 | 1.07e-3 | 7.2872 | 0.889 |
| $e^{\pm}$ | -1.542e-7 | 3.393e-7 | 5.025 | | | | 0.0572 | 0.982 | 37.984 | 2.61e-3 | -27.995 | 0.693 |
| $d, \bar{d}$ | -2.469e-6 | 0.3706 | 21.654 | 5.131e-7 | 30.050 | 0.781 | 0.1311 | -0.971 | 4.691 | | | |

(a)

| PID | $\langle dE/dx\rangle_{\text{Bichsel}} - \langle dE/dx\rangle_{\text{Data}}$ | | | | | | $\sigma(dE/dx)_{\text{Data}}$ | | | | | |
|---|---|---|---|---|---|---|---|---|---|---|---|---|
| | $P_1$ | $P_2$ | $P_3$ | $P_4$ | $P_5$ | $P_6$ | $P_1$ | $P_2$ | $P_3$ | $P_4$ | $P_5$ | $P_6$ |
| $\pi^{\pm}$ | -1.236e-8 | 1.777e-7 | 9.938 | | | | 0.0738 | 16.86 | 39.44 | -1.704e-3 | 6.482 | 0.628 |
| $K^{\pm}$ | 5.49e-10 | -2.732e-6 | 7.712 | | | | 0.0743 | 2.67e-5 | 7.17089 | | | |
| $p, \bar{p}$ | -2.140e-7 | 0.0421 | 48.305 | 7.512e-8 | 15.544 | 0.575 | 0.0779 | 1.822 | 22.4277 | | | |
| $e^{\pm}$ | 6.701e-8 | 3.304e-7 | 7.845 | | | | 0.0678 | 468.9 | 59.4001 | | | |
| $d, \bar{d}$ | -1.631e-7 | 0.0818 | 18.91 | | | | 0.1259 | -0.288 | 3.28733 | | | |

(b)

Table 3.1: Parameters of functions from Fig. 3.2 describing track dE/dx as a function of reconstructed momentum for a few particle species. Units of parameters $P_i$ are such that if one provides momentum in Eq. (3.2) in GeV/$c$ the resultant offset of dE/dx MPV with respect to Bichsel parametrization is in GeV/cm, and the resultant $\sigma$ parameter is unitless.

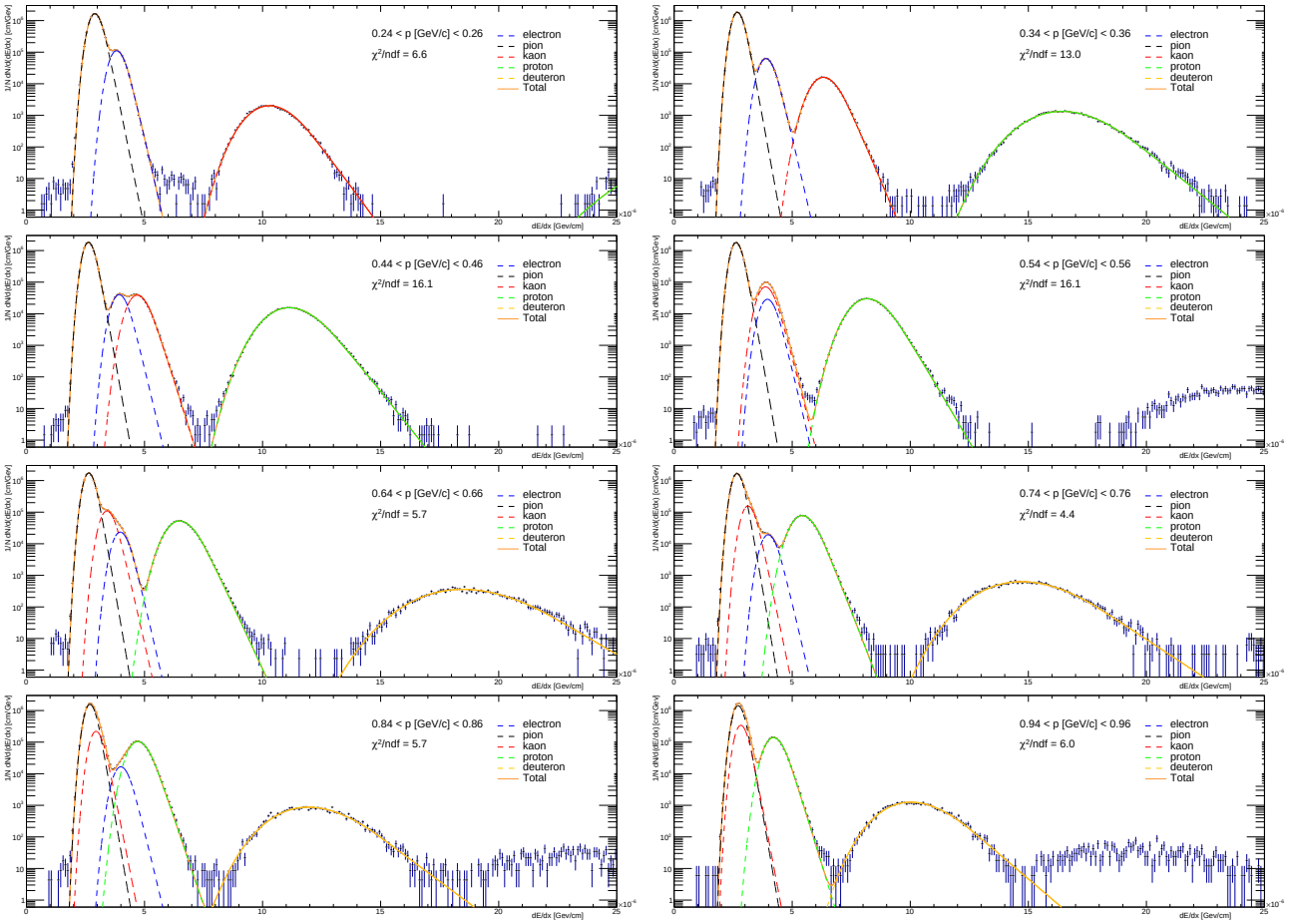


Figure 3.1: Fits of sum of functions from Eq. (3.1) corresponding to different particle species to dE/dx spectra from the data in a few momentum bins.

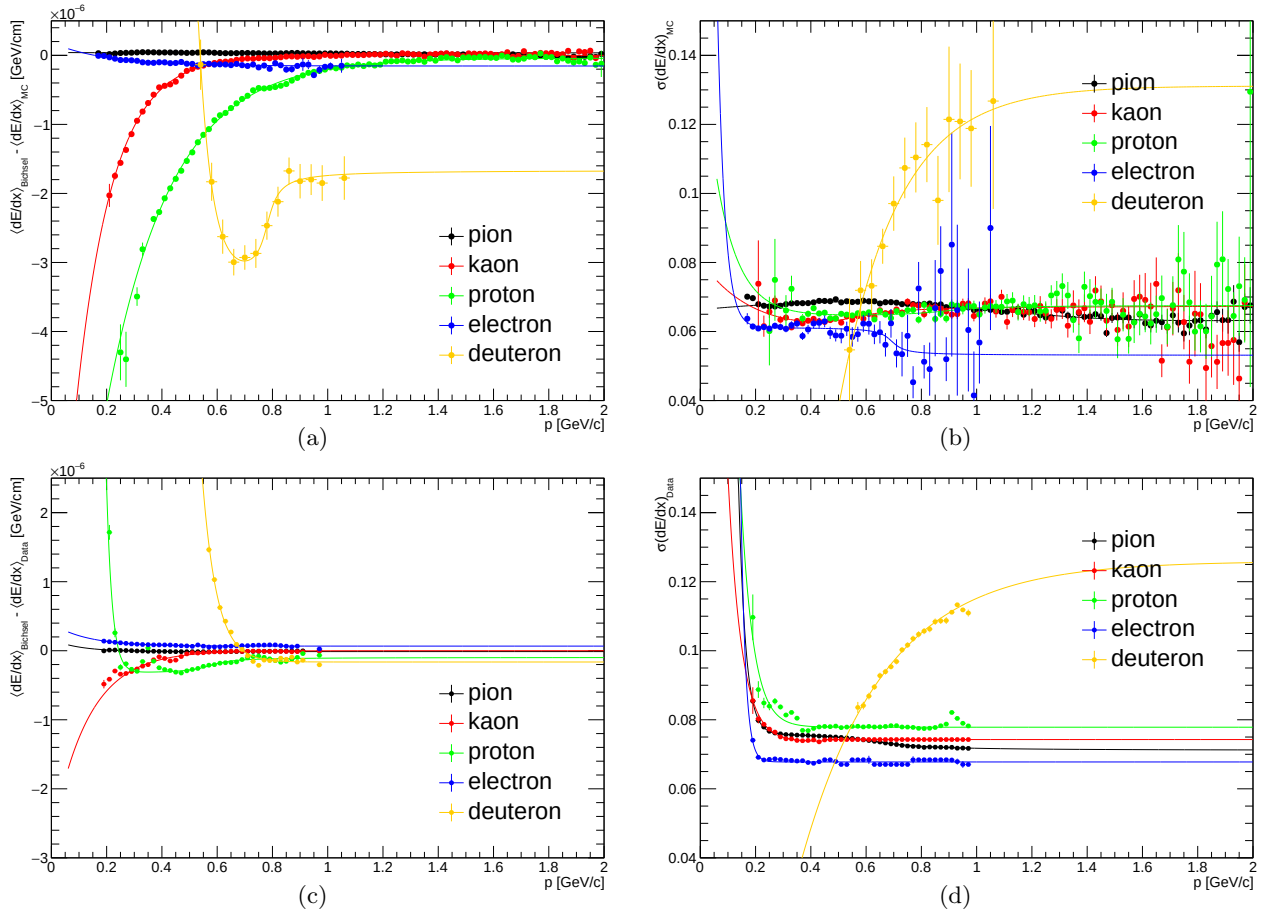


Figure 3.2: Difference between MPV of dE/dx predicted by Bichsel parametrization and obtained from the fit of Eq. (3.1) to dE/dx distribution in the data (3.2c) and MC sample (3.2a) and dE/dx width parameter in data (3.2d) and MC (3.2b) as a function of reconstructed particle momentum for a few particle species. Solid lines represent fits to points of corresponding color.

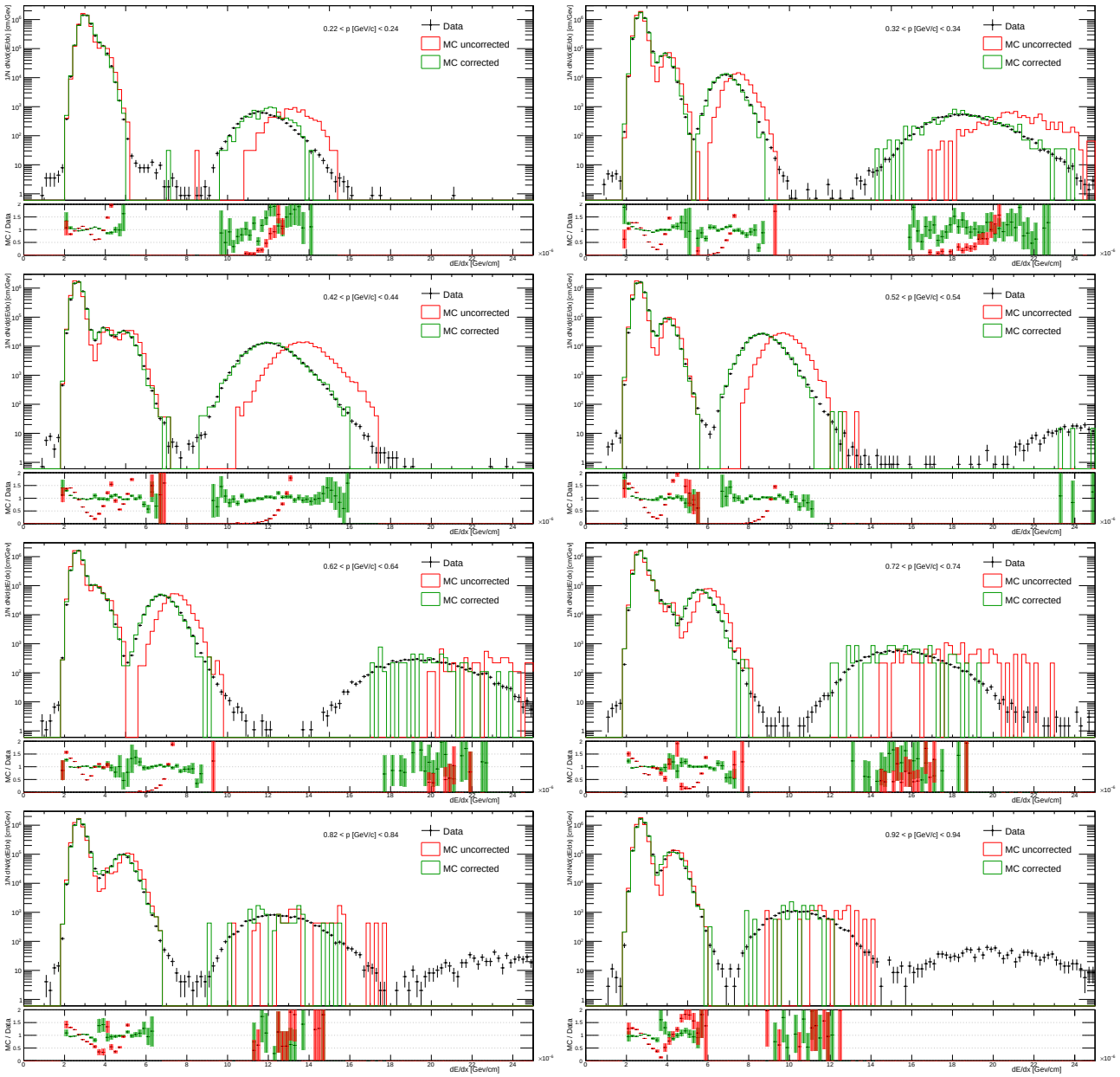


Figure 3.3: Comparison of the dE/dx spectra between the data and MC (before and after correction) in a few momentum bins.

# 4. Dead material in front of TPC

# 5. Systematic errors

# List of Figures



# List of Tables

# References

[1] https://github.com/rafalsikora/CEP-STAR-AnalysisNote/blob/master/CEP_AnalysisNote.pdf.

[2] http://home.agh.edu.pl/~fulek/PID_AnalysisNote.pdf.

[3] S. Das, "A simple alternative to the Crystal Ball function," arXiv:1603.08591 [hep-ex].